NACA RM L56L17

NACA

RESEARCH MEMORANDUM

SOME DATA ON BODY AND JET REACTION CONTROLS

By Allen B. Henning, Andrew R. Wineman,
and Robert W. Rainey

Langley Aeronautical Laboratory
Langley Field, Va.

NATIONAL ADVISORY COMMITTEE
FOR AERONAUTICS

WASHINGTON

March 4, 1957
Declassified February 10, 1959

NACA RM L56L17

NATIONAL ADVISORY COMMITTEE FOR AERONAUTICS

RESEARCH MEMORANDUM

SOME DATA ON BODY AND JET REACTION CONTROLS

By Allen B. Henning, Andrew R. Wineman,
and Robert W. Rainey

SUMMARY

A series of rocket-propelled general-research test missiles incorporating cruciform delta wings, mounted along the diagonals of a fuselage of square cross section, were used to obtain longitudinal trim in flight. These trim characteristics were obtained from several combinations of free-stream and jet-flap controls mounted at fixed deflections at the base of the body. In addition to the effectiveness of these controls, as measured by the change in normal-force coefficient, the static and dynamic longitudinal stability of the test missiles were determined for a range of Mach number of 0.7 to 1.7. Limited tests at a Mach number of 1.62 were made in the Langley 9-inch supersonic tunnel to determine the effects of spoilers mounted on wingless bodies of square and round cross section. Comparisons were made with a conventional, full-span, trailing-edge flap mounted on a delta wing to furnish a reference for the effectiveness of body controls. Effectiveness of three types of reaction controls - immersed jet vane, jet flap, and jet spoiler - have been evaluated and their relative merits discussed. The application of a fin-actuated, jet-vane stabilization system to a Deacon booster rocket was made and flight tested, and the results were analyzed in a qualitative manner.

Sufficient control may be obtained from body-mounted flaps to produce the same trim normal-force coefficient as a conventional flap control mounted on a delta wing, but the required deflections of the body controls would be from 2 to $4\frac{1}{2}$ times as great. Although the trim drag coefficient was from 30 to 70 percent larger, the stability of the model controlled by body flaps was about the same as that of a conventionally controlled model. It appeared that body spoilers have about the same effectiveness as flaps at equal heights above the surface of the body but are not plagued by excessive hinge moments. Of the three types of reaction controls tested the jet spoiler appeared to be the most effective control, based on the amount the thrust vector is tilted for a given impulse loss. As shown by the flight test, immersed jet vanes were used successfully to provide additional lift for fixed booster fins but were also subjected to the wash of the forward wings through the actuating tip control.

INTRODUCTION

In order to maneuver a bomber defense missile toward a target as quickly as possible, large demands are often placed on the missile control system shortly after the missile is launched. Since this type of missile will probably be launched at high altitudes and possibly in a a direction opposite to that of the bomber, the associated low dynamic pressure and negative flight velocities restrict the effectiveness of conventional controls. Because reaction devices furnish control that is not dependent upon ambient conditions, they are therefore applicable to this low dynamic pressure or negative-velocity part of the flight. Jet vanes, jet deflectors, jet spoilers, swiveling nozzles, and similar controls are all classified herein as reaction controls. Information on various reaction controls is reported in various references. (For example, see refs. 1 to 10.) Unless the missile hits the target before the rocket motor is exhausted, additional aerodynamic control is required as the missile closes on the target. If a body-mounted free-stream control can be made to have satisfactory effectiveness, then an advantage in simplicity of attachment and operation can be gained over conventional aerodynamic controls. Thinner airfoil sections with less drag can be employed if the wings are used without attached controls. This idea suggests a composite control system consisting of a reaction control and an aerodynamic control mounted on the body and operated simultaneously by the same servo.

As part of a general research program the National Advisory Committee for Aeronautics has conducted some tests on reaction controls (refs. 11 to 13), but more information on the effectiveness of body controls, both aerodynamic and reaction, is needed. In the present tests, three rocket-powered, delta-wing, general-research missiles were flight tested to obtain the effectiveness of a rocket jet deflector which could also be employed as an aerodynamic body flap control. Square fuselage cross sections were used to facilitate mounting the controls at the base. Results of tunnel tests reported in reference 14 indicate that bodies of square cross section produce higher lift and pitching moment at supersonic speeds than do bodies of circular cross section. Longitudinal trim data, static stability, and dynamic stability of the general-research test missile were determined through the Mach number range of 0.7 to 1.7.

Rocket static tests were made to determine the forces on two jet deflectors, a flap control and a spoiler control. The results of these tests, in turn, initiated limited supersonic-tunnel tests of an aerodynamic spoiler mounted at the base of the body. Limited data from a flight test of an angle-of-attack stabilized booster system employing immersed jet vanes is also presented. Data from all these tests were correlated into four main groups: flap controls, spoiler controls, rocket static test comparisons, and booster stabilization.

All flight tests were conducted at the Pilotless Aircraft Research Station at Wallops Island, Va. Supersonic-tunnel tests were conducted at the Langley 9-inch supersonic tunnel, and rocket static tests were made at the Langley rocket test cell.

SYMBOLS

A_s control area projected to the nozzle exit

A_e nozzle exit area

$\bar{c}$ mean aerodynamic chord, ft

C_A axial-force coefficient, $\frac{\text{Axial force}}{qS}$

C_D drag coefficient, $C_N \sin \alpha + C_A \cos \alpha$

C_m pitching-moment coefficient, $\frac{\text{Pitching moment}}{qS\bar{c}}$ and $\frac{\text{Pitching moment}}{(\text{Body cross-sectional area})\ qd}$

C_N normal-force coefficient, $\frac{\text{Normal force}}{qS}$ and $\frac{\text{Normal force}}{(\text{Body cross-sectional area})\ q}$

C_L lift coefficient, $C_N \cos \alpha - C_A \sin \alpha$

C_p pressure coefficient, $\frac{p_m - p}{q}$

C_{L_α} slope of lift curve, $\frac{dC_L}{d\alpha}$, per deg

$C_{m_q} + C_{m_{\dot{\alpha}}}$ damping-in-pitch derivative, $\frac{dC_m}{d\left(\frac{q\bar{c}}{2V}\right)} + \frac{dC_m}{d\left(\frac{\dot{\alpha}\bar{c}}{2V}\right)}$, per radian

d diameter of body with circular cross section or width of body with square cross section, ft

h	height of control, ft
I_Y	moment of inertia in pitch, slug-ft^2
M	Mach number
M_e	Mach number at exit of rocket nozzle
p	static pressure, lb/sq ft
p_m	manifolded pressure of three flap orifices, lb/sq ft
p_s	standard sea-level static pressure, 2,116 lb/sq ft
q	dynamic pressure, $0.7pM^2$, lb/sq ft; or pitching velocity, radians/sec
R	Reynolds number, $V\bar{c}/\mu$
S	total wing area in one plane, sq ft
t	time, sec
$t_{1/2}$	time for an oscillation to damp to one-half amplitude, sec
V	velocity of model, ft/sec
W	weight of model, lb
x	distance from leading edge of $\bar{c}$, or distance from apex of body nose, ft
α	angle of attack, deg
$\dot{\alpha}$	$\frac{1}{57.3}\left(\frac{d\alpha}{dt}\right)$, radians/sec
β	angle of sideslip, deg
δ	angle of control deflection, deg
δ_α	angle of jet-vane deflection in pitch plane, deg (positive α produces negative δ_α)

δ_β angle of jet-vane deflection in yaw plane, deg (positive β produces negative δ_β)

μ coefficient of viscosity, slugs/ft-sec

Subscripts:

1 aerodynamic flap

2 jet flap

ac aerodynamic center

cp center of pressure

trim trim condition, $C_m = 0$

MODELS

Three models (called model 1, model 2, and model 3) were used to evaluate the effectiveness of body-mounted flap controls. A typical model (model 3) is shown in the sketch of figure 1, and the photographs of models 1, 2, and 3 are shown in figure 2. The geometric characteristics of the three models were identical except for the two controls. The different combinations of control settings tested are shown in figure 3. A 5-inch British Cordite rocket motor, incorporated in the model as a second-stage motor, was delayed in ignition until the model had coasted through the Mach number range. After the second-stage motor burned out, the models again coasted through the same Mach number range but at different weights, inertias, and center-of-gravity locations. The mass characteristics of models 1, 2, and 3 are given in table 1.

The fuselage of each model consisted of a parabolic nose with a straight afterbody. The cross section of the body was circular at the nose but was developed into a square cross section by using a 17-inch transition. Flat-plate, cruciform, 60° delta wings with beveled leading and trailing edges were mounted on the corners of the body having square cross section just rearward of the transition. Flap controls were mounted on all sides of the base of the square body, but only those in the pitch plane were deflected for these tests. The upper control, referred to hereinafter as an aerodynamic flap, was always deflected into the airstream; the lower control, which shall be called a jet flap, was deflected into the jet exhaust of the rocket motor.

The deflection of both the aerodynamic flap and the jet flap of model 1 remained fixed for the duration of the flight. However, for

models 2 and 3 the deflection of the jet flap was changed in flight by use of a position servo (figs. 1(b) and 1(c)) utilizing rocket chamber pressure. This servo mechanically locked the jet flap at zero deflection for the duration of the first coast; however, when the rocket motor in the model ignited, this servo deflected the flap into the rocket jet at a predetermined angle and again locked it at this new position for the remainder of the flight. The area of the flap impinged by the jet for these two deflections is shown in figure 1(d). Model 3 was equipped with four rockets, each having an impulse of 6 pound-seconds and were aimed to disturb the model in the pitch plane.

The sketches and descriptions of the supplementary test models such as the static-test models, the wind-tunnel models, and the immersed-jet-vane, free-flight model are presented subsequently.

INSTRUMENTATION AND TESTS

Each model was equipped with a standard NACA four-channel telemeter transmitter which conveyed a continuous signal from the model to ground stations. The instruments of models 1 and 2 measured normal and longitudinal accelerations, total pressure, and a sample pressure on the aerodynamic flap. This flap pressure was measured by means of three manifolded holes located on the longitudinal center line of this control. Model 3, which was disturbed in pitch, was instrumented to measure angle of attack, normal and longitudinal accelerations, and total pressure. Normal and longitudinal accelerometers were located in the nose section just forward of the transition section of the model. Flight Mach number was determined by the use of measured total pressure and data from the following: an NACA modified SCR-584 tracking radar, a rawinsonde, and a CW Doppler velocimeter.

After each model was accelerated to supersonic speeds by a solid-propellant Deacon booster rocket, it was subjected to three different flight conditions: first, decreasing velocity after seperation from the booster; second, increasing velocity to supersonic Mach numbers for power on; and, finally, decreasing velocity again to subsonic speeds during the second coast. This double-coast method was initially used to furnish a check on trim data of the test configuration for different altitudes at a constant control deflection. However, since this check between the data of the first and second coasts was established by the flight test of model 1, the deflection of the jet flap of models 2 and 3 was changed in flight as the second-stage rocket motor ignited. Thus, the test conditions between the first and second coasts of models 2 and 3 were changed by increasing the control deflection of the jet flap. Deflecting this control into the rocket jet also provided longitudinal trim data during the power-on part of the flight. The test Mach number range of 0.7

to 1.7 was approximately the same at each of three flight conditions - first coast, second coast, and power on for all three models. Reynolds numbers of the tests are shown in figure 4, and the ratio of static pressure to standard sea-level pressure is shown in figure 5.

Instrumentation and test procedure of the static tests, wind-tunnel tests, and the additional flight test are described in the "Discussion" of this paper.

REDUCTION OF DATA

For the models which were not disturbed in flight and which were used only to determine longitudinal trim at various control settings, the data reduction consisted in merely converting measured normal and longitudinal accelerations to normal-force and axial-force coefficients. However, one model was disturbed in pitch by pulse rockets during the first coasting period of the flight in order to determine the longitudinal static and dynamic stability of the configuration. These stability data were evaluated by use of the equations of motion for two degrees of freedom and the transients of the free motions of the flight model resulting from pitch disturbances. A detailed discussion of this method of flight-data analysis may be found in the appendix of reference 15. This method of reducing the data pertains only to models 1, 2, and 3. Data reduction of the remaining tests is discussed subsequently.

ACCURACY

The precision of the measured data is often difficult to determine, and only estimates of the accuracy can be made. Repeatability of test data is sometimes used as a standard of accuracy; however, when the data are determined from flight models where this is impractical, the precision of the measured data and the reliability of the calculated final data are usually determined by experience and possible mathematical estimates. For the flight models reported herein, the accuracy of the data was estimated by using the method of probable errors as demonstrated in reference 16. The probable errors of the direct measuremements were chosen to be $\pm 1/2$ percent of the calibrated instrument range. Probable errors of the final data were then calculated by equation 139.1 of reference 16. This equation states that the probable error is the square root of the sum of the squared products of the probable error of individual direct measurements and the partial derivative of the final result with respect to these direct measurements. Probable errors of the presented data from flight tests of the square body configurations are shown in table II along with estimated errors of static tests, tests from the Langley 9-inch supersonic tunnel, and the flight test of the immersed-jet-vane booster.

RESULTS AND DISCUSSION

No parameter alone can be employed to evaluate the usefulness of a certain control. Control effectiveness itself is a function of three nearly independent variables: control lift, the location of the control with respect to the aircraft center of gravity, and the static stability of the aircraft. Other parameters such as drag and servo power dictate the applicability of a control to a specific configuration. However, before a control is adopted, it must first demonstrate sufficient effectiveness to change appreciably the trim of an aircraft in flight. Thus, the longitudinal trim at various deflections and the stability of a test vehicle were measured in flight to determine the effectiveness of body-mounted flaps. Wind-tunnel and rocket static tests were also utilized to determine some relative merits of body-mounted spoilers and jet-deflection controls. Qualitative information on a booster stabilization system is discussed.

Paddle Controls

Trim.- The trim normal-force data of all three models are presented as coefficients in figure 6. The trim lift coefficient of model 3 is also presented in figure 6, and the corresponding trim angle of attack is shown in figure 7. Except for the transonic regions, there were no unusual variations of these trim parameters with Mach number, and they were also fairly linear with flap deflection. As mentioned previously, the deflections of both controls of model 1 remained constant throughout the entire flight. The Reynolds number between the first and second coast was different, as shown in figure 4; and there was an apparent influence of the rocket jet on the afterbody of the model during the power-on part of the flight. However from all parts of figure 6 it can be noted that only slight differences in the trim normal-force coefficient were detected between the three flight conditions of model 1. Since these differences were less than the accuracies of the test data, as shown in table II, the influence of Reynolds number and jet effects on model trim were considered insignificant. The trim normal-force coefficient of the second coast of models 2 and 3 was increased over that of the first coast by 25 to 50 percent. This increase was directly attributed to the deflection of the jet flap which, when deflected in conjunction with the aerodynamic flap, produced a cambered-afterbody effect. The effect of rocket power on the jet flap increased the trim normal-force coefficient an additional 10 to 100 percent over that of the second coast. This corresponds to an increase in trim during power on from $\frac{1}{3}$ to $2\frac{1}{2}$ times that of the first coast. This increase in trim during power on is directly attributed to the control moment obtained as the jet flap deflects the high-energy jet of the rocket motor from

the center line of the model. As shown in figures 6(b) and (c), larger changes in model trim were experienced at the lower dynamic pressures at subsonic speeds. This fluctuation is not an unusual trend for a model employing reaction controls, since the aerodynamic restoring moments of the model decrease directly with the dynamic pressure; however, the control moment is independent of ambient conditions and remains nearly constant with flight Mach number.

The absolute values of trim and flap deflections are more significant when compared with conventional controls of known characteristics. Here the deflection was used as a tool for comparing the effectiveness of controls, although it is realized that other parameters are involved, such as hinge moments, servo power, and control drag. Such a comparison was made by using the wing-body combination of reference 17 that incorporated a full-span, unbalanced, trailing-edge control mounted on a triangular wing of aspect ratio 2. This control had about twice the area and one-half the tail length of the control of model 3. After the data of reference 17 were converted to the various center-of-gravity locations of model 3, the deflections required by the full-span flap to produce the same trim lift coefficients were then calculated and are shown in the following table for a supersonic and a subsonic Mach number.

Mach number	Flight condition of model 3	Deflection required of reference control to produce same trim as model 3, deg
1.5	First coast	9.1
1.5	Second coast	11.5
1.5	Power on	16.6
0.8	First coast	4.7
0.8	Power on	11.1

From this table it is noted that the deflections required of the reference control to produce the same trim lift coefficient as model 3 are all less than the deflection of the aerodynamic flap ($\delta_1 = 21.83^\circ$). For power off, or during first and second coast, the deflection required of the reference control was only 22 to 50 percent of that required by the aerodynamic flap. Similarly for power on, when both the aerodynamic flap and the jet flap were deflected 21.83°, the reference control required 51 to 76 percent of this deflection. This indicates that for the same trim the aerodynamic flap would require from 2 to $4\frac{1}{2}$ times the deflection of a full-span, trailing-edge control mounted on a delta wing. An increase of 30 to 100 percent over this conventional control was also

apparent when the effectiveness of the jet flap was included with the aerodynamic flap in the comparison. It is interesting to note, from the preceding table, that the reference control would require about 90 percent more deflection at $M = 1.5$ than at $M = 0.8$ to produce the same trim lift as model 3. This indicates that the effectiveness of the aerodynamic control of model 3 is more constant with Mach number than the effectiveness of the reference control.

The effectiveness of the jet flap, as determined from rocket-static-test data, was used in conjunction with the power-off flight data to predict the model trim characteristics during power on. A jet flap and a rocket motor similar to those employed on the flight model were statically tested. A sketch of this control and a summary of the data are presented in figure 8. These data were obtained by continuously pulsing one of the jet flaps in a sinusoidal manner over a deflection range of 0° to 25° into the jet exhaust of a standard 5-inch British Cordite rocket motor. Thrust, chamber pressure, normal force, pitching moment, hinge moment, and flap deflection were measured continuously throughout the test. The nozzle was extended for both the static test and the flight test to improve the rocket performance and facilitate mounting the jet flap.

Because the arrangement of the flaps used in the static test was geometrically similar to the afterbody of the flight model, it was estimated that the jet flap did not enter the jet until it had deflected about 10° from the body contour; actually zero normal force and hinge moments were measured at $\delta = 13.5^\circ$. The jet-flow deflection, or the amount the jet flap tilted the thrust vector, was determined directly from the ratio of measured normal force to thrust, and the impulse loss was obtained from the variation of thrust with flap deflection. Although the normal force and thrust changed during the burning of the rocket motor, the flow deflection remained nearly constant. Normal force and hinge moment were averaged for the burning time of the rocket motor and are included in figure 8 only to indicate the magnitude of these parameters. Knowing this normal force and the approximate center of pressure of the jet flap made it possible to estimate the contribution of the jet flap to the trim characteristics of models 2 and 3.

A comparison of this estimate with the measured power-on data of the flight models is shown in figure 9, and good agreement is noted for supersonic Mach numbers. However, at lower Mach numbers the estimated values of both the trim angle of attack and the normal-force coefficient are less than the corresponding trim parameters as measured in flight. Since only the jet flap was pulsed during the static test, any additional flow deflection of the rocket jet that would result from the aerodynamic flap moving in unison with this control was not measured, but this condition was included in the power-on data obtained from flight tests. Therefore, the estimated trim should be less than the measured trim because the

jet-control moment is independent of dynamic pressure. This difference in trim would be amplified at the lower Mach numbers because the control moment remains nearly constant with Mach number, but the aerodynamic moment decreases.

Flap pressure coefficient.- In order to gain some knowledge of the pressure forces on the aerodynamic flap, a sample pressure was measured from three manifolded orifices located along the longitudinal center line of the control. The data are presented as pressure coefficients in figure 10 for the first coast, second coast, and power-on conditions of models 1 and 2. Also presented in figure 10 is the theoretical pressure coefficient for a two-dimensional flat plate deflected 6.44° behind an oblique shock. Theoretically, the shock caused by the deflected control is detached at Mach numbers less than 1.3 for model 1 and 1.7 for model 2. Although there is fair agreement between the theoretical and experimental pressure coefficients of model 1, the measured values obtained from the first coast of the flight are appreciably lower than those obtained during the second coast and power-on phases of this flight. Because of the small control deflection of model 1 ($\delta_1 = 6.44°$ or $h/d = 0.06$) the boundary layer and the detached shock were believed to have caused this difference. As the aerodynamic flap was deflected to a larger angle ($\delta_1 = 16.78°$ or $h/d = 0.17$), it seemed to be in a more stable flow region, which is indicated by the excellent agreement of C_p at supersonic speeds during the three different flight conditions of model 2. The largest measured value of C_p for both model 1 and model 2 occurred at $M = 1.2$ and was about 0.3 and 0.4, respectively.

Axial-force and drag comparison.- The axial-force coefficient is presented in figure 11 for all three models during the first coast and for models 1 and 3 during the second coast. The axial-force coefficient was not presented for the second coast of model 2 because of a questionable shift in the accelerometer data after burnout of the rocket motor. The trim axial-force coefficients resulting from the deflected aerodynamic flap alone are shown in figure 11(a), and the corresponding axial-force coefficients resulting from the simultaneous deflection of both the aerodynamic flap and the jet flap of model 3 are shown in figure 11(b). It is believed that the minimum drag of the configuration is of approximately the same magnitude as the axial-force coefficient of model 1 ($\delta_1 = 6.44°$, $\delta_2 = 0°$). The axial-force coefficient from the first coast of this model varied from 0.04 to 0.07 and agreed favorably with the second-coast data. Deflecting the aerodynamic flap from 6.44° to 16.78° increased C_A from 4 to 15 percent at supersonic speeds and about 24 percent at subsonic speeds. Deflecting the control still farther (from $\delta_1 = 16.78°$ to $\delta_1 = 21.83°$) produced very little change in C_A at subsonic and supersonic speeds, but because of an earlier drag rise an

increase of 10 to 15 percent was noted at transonic speeds. Within the accuracy of the data, the effect of deflecting the jet flap in unison with the aerodynamic flap did not appear to influence the magnitude of the axial-force coefficient at supersonic Mach numbers. Since the angle of attack was measured for model 3, lift and drag coefficients could be determined; however, the pulse rockets did not disturb the model sufficiently to obtain the lift coefficient for minimum drag.

The drag coefficient for trim lift is presented in figure 12 for both the first and second coasting periods of this model. The total drag coefficient of a somewhat similar configuration was obtained from the lift-drag polars of reference 10 for a lift coefficient equal to the trim lift of model 3, and it is also presented for comparison in figure 12. The reference model had cruciform wings of the same plan form as the present model with tip controls deflected 10°, a fuselage of the same fineness ratio but with a circular cross section, and a boattailed afterbody. Although it is realized that the boattail of this model was a factor used to reduce total drag, a comparison is made in figure 12 between two configurations which could perform the same mission. The drag coefficient at trim lift of model 3 was greater than the drag coefficient of the reference model by about the same percentage for the first and second coasts, 30 percent greater at supersonic speeds, and 60 to 70 percent at transonic and subsonic speeds. Differences between the drag coefficients of the first and second coasts is attributed to the differences in trim angle of attack shown in figure 7.

Stability.- As mentioned previously, the static and dynamic longitudinal stability of model 3 was measured from free oscillations caused by pulse rocket disturbances during the first coasting period of the flight. An additional disturbance was attained as an outcome of deflecting the jet flap into the rocket exhaust immediately after the second-stage motor ignited. The measured lift-curve slope and the location of the aerodynamic center of this configuration are presented in figure 13, and data from the flight model of reference 18 are also included for comparison. Throughout the test Mach number range C_{L_α} varied from about 0.04 to 0.05 per degree and agreed within 5 percent of the reference model at supersonic speeds. The limited lift-curve slopes with power on showed favorable agreement with the power-off data in the transonic speed range, although data from the first cycle of the power-on disturbance indicated a larger slope at a subsonic Mach number. The aerodynamic center moved rearward on the model nearly linearly with Mach number from subsonic speeds to $M = 1.3$, and then moved forward slightly as shown in figure 13(b). The total movement of the aerodynamic-center location was about 16 percent $\bar{c}$, or twice that of the reference model. Compared with data of reference 18, the aerodynamic center of model 3 at supersonic speeds was rearward of the reference model by as much as 6 percent $\bar{c}$, thus an effect of the afterbody having a square cross section and possibly the body controls on the static stability was indicated.

An indication of the dynamic stability of model 3 is shown by the magnitudes of the time for the model to damp to one-half amplitude (fig. 14(a)) and the damping-in-pitch derivative $C_{m_q} + C_{m_{\dot{\alpha}}}$ (fig. 14(b)). The damping-in-pitch derivative $C_{m_q} + C_{m_{\dot{\alpha}}}$ had a maximum value of about -6 at $M = 0.8$ and averaged approximately -3 at supersonic speeds. Although these low values of damping are not uncommon for tailless missiles, as shown in reference 19, the damping in pitch of model 3 was consistently larger than the similar model of reference 18. It is believed that the square fuselage of model 3 contributed a large percentage of the increase in $C_{m_q} + C_{m_{\dot{\alpha}}}$ over the reference model, especially at subsonic speeds.

Spoiler Controls

Because the hinge moments of flap controls can become quite large, as in figure 8, and may require unreasonable amounts of servo power at operational deflections, the effectiveness of a spoiler placed on the base of the body became of interest. To establish qualitatively the effectiveness of body-mounted spoilers which would operate both as an aerodynamic control and a jet control, a test was made in the Langley 9-inch supersonic tunnel on an aerodynamic body spoiler. Limited data were also obtained from a static test on a spoiler used to deflect the jet of a rocket motor. These data were combined with the stability data obtained from model 3 to calculate estimates of the trim characteristics of a model geometrically similar to model 3 but controlled by body spoilers. Estimates obtained in this manner were compared with the measured trim of model 3 for both power-on and power-off conditions.

Wind-tunnel tests.- The normal force and pitching moment of two wingless bodies, one with a square cross section and one circular, were measured in the 9-inch supersonic tunnel both with and without spoilers mounted at the base. The models, as shown in the sketch of figure 15, were magnesium bodies having a ratio of length to diameter of 10 with a parabolic nose and a cylindrical afterbody. A transition strip of powdered aluminum oxide was attached on the forward section of the nose, and spoilers of two different heights ($h/d = 0.25$ and $h/d = 0.50$) were mounted flush with the base. The test was made at a Mach number of 1.62, a Reynolds number 5.7×10^6, and a nominal range of angle of attack of -6° to $+8^\circ$. No axial force was measured since the models were designed to use an existing two-component balance. Schlieren photographs of both the square and circular bodies at angles of attack near $\frac{1}{2}^\circ$ and 9° are also presented in figure 15 to indicate the flow phenomena in the vicinity of the spoiler. Pitching-moment and normal-force coefficients, referred to body length and cross-sectional area, are shown in figure 16 for both square and circular bodies with and without spoilers.

The contribution of the spoiler to the characteristics of the basic bodies was obtained from these data and is presented in figure 17. It was believed that the effectiveness of the spoiler could best be described as the incremental change in normal-force coefficient ΔC_N and the longitudinal location of its line of action with relation to the basic body. The normal-force coefficient and center of pressure of the basic body are shown in figures 16 and 17(a), respectively, and the isolated effect of the spoiler is shown in figure 17(b). The center of pressure of the control force of both bodies for a value of h/d of 0.25 was very close to the base and also remained nearly constant with angle of attack. The change in normal-force coefficient for the spoiler mounted on the square body was about 25 percent more than that obtained from the circular body. This difference in ΔC_N was increased to about 45 percent as the spoiler heights were changed from 1/4 to 1/2 of the body diameter; and although the center of pressure remained close to the base of the square body, it moved rearward of the body and also varied with angle of attack for the circular body. The movement of the center of pressure of the larger spoiler on the circular body may have resulted from the influence of the spoiler area which extended into the free stream beyond each side of the body, as shown in the sketch in figure 17(b). Even when this rearward movement of the center of pressure and the fact that the exposed spoiler area of the circular body was nearly 20 percent greater than that of the square body for an h/d of 0.5 are taken into consideration, the effectiveness of the spoilers was consistently better when used in conjunction with the body of square cross section. It is also interesting to note (fig. 16) that the slope of the normal-force coefficient of the square body without the spoiler was nearly 30 percent larger than that of the corresponding circular body at an angle of attack of 0°. Similarly, for a square body with slightly rounded corners, a 20-percent increase in C_{L_α} was noted when comparison was made with a corresponding circular body at $M = 2.01$ in reference 14. However, from the present tests, nonlinearities with angle of attack were discovered in both the control force and control moment; larger variations were indicated for spoilers mounted on square bodies. Therefore, body spoilers should be used with caution when they are employed on wingless bodies or body-wing combinations which fly at low static stability for ease of control because nonlinearities in control effectiveness could cause very large trim changes or even divergent aircraft motions, although the configuration may be statically stable at zero control deflections.

Rocket-jet tests.- Some indication of the effectiveness of body-mounted spoilers, while deflected into the exhaust of a rocket motor, or jet spoilers was obtained from the static tests of five standard 3.25-inch MK 7 rocket motors with plates of various sizes welded over a small portion of the nozzle exit, as shown in the sketch of figure 18.

Normal force and thrust were obtained from an average of continuous measurements made during the burning time of the rocket motor. Flow deflection angle, or the arc tangent of the ratio of measured normal force to the measured thrust, was used to indicate effectiveness of the control at different ratios of spoiler area to nozzle exit area. The thrust penalty caused by the spoilers is shown by the loss of thrust impulse as compared with the total impulse of the rocket motor without spoilers. For example, a 4-percent loss in impulse was noted as the jet was deflected 5°. Since in practice there is some gap between the spoiler and the rocket nozzle, the spoiler on one motor was welded only at the ends, rather than around the outside edge, to allow a gap between the spoiler and nozzle. As shown in figure 18, the spoiler control moment varies nearly linearly with the blocked nozzle area. This nearly linear variation coupled with the low impulse losses indicates, for the range of the present test, that the jet spoiler is an effective means of control. However, if a gap between the spoiler and nozzle of about 6 percent of the nozzle exit diameter is present, which is probably large for most practical applications, a 35-percent loss in normal force results. The loss in rocket impulse is more than twice the loss associated with the spoiler without the gap. Because both the normal force and thrust decrease together, the deflection of the resultant thrust vector is reduced only about 10 percent.

Relative merits of flap and spoiler controls.- In order to determine the relative effectiveness of spoiler controls compared with flap controls when mounted at the base of a body, the trim angle of attack and the trim normal-force coefficient of a spoiler-controlled model similar to model 3 were estimated for the power-on and power-off conditions at $M = 1.62$ and were then compared with the measured trim characteristics of the flap-controlled flight models in figure 19. The power-off trim of the spoiler-controlled model was established from ΔC_N of the spoiler, center of pressure of the spoiler, and the static stability of model 3. The data for the spoiler on the square body for $h/d = 0.25$ and $h/d = 0.50$, as determined by the wind-tunnel tests, were taken from figure 17(b); lift-curve slope and the aerodynamic center location of model 3, as determined from the flight-test data, were taken from figure 13. Estimates of the power-on trim of the spoiler-controlled model were obtained by combining the calculated power-off trim with the effects of the jet spoiler as obtained from figure 18. The effectiveness of the jet spoiler was also determined by the amount the average thrust of a 5-inch British Cordite rocket motor could be tilted with a spoiler that blocked about 10 percent of the nozzle-exit area, or the same areas as blocked by the jet flap when deflected 21.83°. It was assumed that the center of pressure of the control was at the longitudinal location of the spoiler, and the contribution of the reaction control to the power-off trim data was then calculated for the hypothetical spoiler-controlled model.

The comparison of the estimated trim of a spoiler-controlled model with that of a flap-controlled model is presented in figure 19. When the aerodynamic body spoilers were mounted on a model equivalent to model 3, figure 19(a) shows that the trim angle of attack and trim normal-force coefficient were both estimated to be larger than the values for the same model controlled by an aerodynamic flap deflected 21.83° - about 35 percent larger for a spoiler deflection of $h/d = 0.25$ and more than twice as large for $h/d = 0.50$. Adding the effect of the jet spoiler ($h/d = 0.16$) to the increment contributed by the aerodynamic spoiler ($h/d = 0.25$), a 38-percent increase in trim angle of attack was noted over the power-on data of the flap-controlled model, and about a 30-percent increase was also noted in the normal-force coefficient. The large aerodynamic spoiler, with a height of one-half the body diameter or nearly as high as the aerodynamic flap when deflected 90° ($h/d = 0.54$), is probably the maximum height that can be used in practice from a structural standpoint and can be considered as the upper limit of the power-off trim of the spoiler-controlled model. Because calculations indicate that the flap of model 3 operated behind a detached shock wave at Mach numbers less than 1.7, it is reasonable to expect that the spoiler, which theoretically detaches the shock to some extent for all supersonic test Mach numbers, produces similar trends with Mach number, at least for values greater than $M = 1.0$.

Since only two sizes of the aerodynamic spoilers were tested and neither was directly comparable with the aerodynamic flap, only qualitative comparisons of the effectiveness could be obtained from the trim characteristics. Figure 19(b) shows the variation of the trim normal-force coefficient of models 1, 2, and 3, extrapolated to $M = 1.62$, and the estimated trim values obtained from a spoiler-controlled model as a function of the height of each control above the surface of the flat fuselage. For the configuration investigated, the trim normal-force coefficient resulting from the aerodynamic body spoilers varied with h/d in a manner very similar to the aerodynamic flaps, and it appeared that the effectiveness of the two types of control was about equal at corresponding heights above the fuselage. If this apparent equality is true, then body spoilers offer a means of control that is as effective as body flaps but without the penalty of the large hinge moments for control deflections up to one-half the height of the body.

Rocket-Static-Test Comparisons

Three types of reaction controls used to deflect the rocket exhaust from the longitudinal center line were statically tested: the jet flap shown in figure 8, the jet spoiler shown in figure 18, and an immersed jet vane presented in reference 13. Data from these tests were correlated and are presented in figure 20 as a summary and a comparison of the relative merits of the three types of jet controls. The ultimate

purpose of these controls is to obtain a maximum deflection of the thrust vector with a minimum loss in thrust impulse; therefore flow deflection angle and percent loss in impulse due to control drag were used as basic parameters for comparison. Although the normal force and hinge moments are presented, quantitative comparisons of these data can not be made directly because in each of the three types of tests there were such factors as various rocket motors of different thrusts, nozzle characteristics, and burning durations. A 5-inch British Cordite rocket motor was used with the jet flap, a $3\frac{1}{4}$-inch aircraft rocket motor was used for the jet spoiler, and a 6.25-inch Deacon rocket motor was used for the immersed jet vane. Because all controls differed in size and because deflections of spoiler, flap, and vane controls were not compatible, the amount of area blocked by the control in percent of the nozzle exit area was used as the independent variable for these comparisons. For the jet flap and the immersed jet vane, where the control was not in the plane of the nozzle exit, the blocked area A_S was obtained by projecting the control area onto the nozzle exit plane along perspective rays originating from the geometric apex of the nozzle cone. The magnitude of the hinge moments should not be compared directly because no attempt was made to reduce the hinge moments of the jet flap, but such an attempt was made in the tests of the immersed jet vane. Although hinge moments were not measured on the jet spoiler, they were not considered because actuation devices for spoilers generally produce a variable area rather than a variable deflection of hinged controls.

It is evident from figure 20(a), for the range of the measured data, that the jet spoiler was more effective in turning the flow of the rocket exhaust gases than either the immersed jet vane or the jet flap. All three controls exhibited a nearly linear variation of effectiveness, or flow deflection, with blocked area except the jet flap for areas less than 4 percent of the nozzle exit area. Although the jet spoiler deflected the flow about $1\frac{1}{2}^\circ$ more than the jet flap at equivalent blocked areas, the thrust impulse loss of the two controls was nearly the same. However, with a relatively large gap of 6 percent of the nozzle exit diameter, the effectiveness of the spoiler was reduced about 10 percent, but the impulse loss was more than doubled. The flow deflection of the immersed jet vane, at the maximum vane deflection of 12.5°, was a little more than 1° or about one-half of that obtained by the jet spoiler for the same area blocked by the control. However, a penalty of 2-percent loss in impulse is associated with the immersed jet vane at zero deflection, but this loss was not encountered with either the jet flap or the jet spoiler at equivalent areas.

A summary of the relative merits of the three types of reaction controls tested, which is essentially control drag as a function of control effectiveness, is shown in figure 20(b). For an impulse loss of 2 percent the immersed jet vane tilted the thrust vector about 1°, the jet

flap about 3°, and the jet spoiler without a gap about $4\frac{1}{2}°$. However, to turn the flow $4\frac{1}{2}°$ with a jet spoiler that includes a relatively large gap between the spoiler and the nozzle, the impulse losses may increase fourfold.

Booster Stabilization

The booster used to accelerate a missile to supersonic speeds often requires large fixed fins to stabilize the model-booster combination during the first phase, or the boosted part, of the flight. Because the center of gravity of the combination moves forward as the rocket fuel is expended, the static-stability requirement at subsonic speeds often dictates the size of the booster fins. Since the force produced by a reaction control is independent of ambient conditions, jet vanes can be used advantageously to furnish the necessary force required for stabilization of a model-booster combination at low speeds; however, additional fixed fins are often required for the high-speed phase of the flight because the load on the model increases in proportion to the square of the velocity, whereas the effectiveness of the jet vane is independent of the velocity. A booster employing this arrangement of fixed fins and reaction controls should have better performance than the same booster with fixed fins alone. As shown in reference 12, a free-floating fin could be used in conjunction with immersed jet vanes of very low hinge moment to produce a control force in the same direction as the lift forces of a fixed booster fin. The size of the fixed fin, when used with a fin-actuated jet-vane stabilization system, is determined at the higher velocity phase of the flight by the difference between the destabilizing effect of the model on the combination and the stabilizing force of the jet vane.

In order to evaluate the application of a booster employing jet vanes sensitive to angle of attack, a booster for a flight model was designed with fixed fins and immersed jet vanes to furnish additional stability in both the pitch and yaw planes. Immersed vanes were chosen because of the simplicity of their application to Deacon rocket motors and the availability of the static test data of reference 13. Pertinent characteristics of the flight model are shown in figure 21. The wings of the model were cruciform, 60° delta flat plates with beveled leading and trailing edges, and they were mounted on a cylindrical 7-inch-diameter body with an ogive nose section. The model was directly attached to the forward end of the 6.25-inch Deacon rocket motor. In contrast to almost all booster combinations, the forward section of this model was designed not to separate from the booster rocket motor after its fuel was exhausted.

The tail of this model (fig. 21) or the simulated booster fins consisted of 45° delta, flat-plate, cruciform fins with beveled leading and trailing edges incorporating tip controls to actuate immersed jet vanes. The 45° delta tip control was hinged at 10 percent $\bar{c}$ ahead of the leading edge of the mean aerodynamic chord of the control and actuated the immersed jet vane which was hinged at $0.38\bar{c}$ by a mechanical linkage, rack, and gear, with a gain of 3 to 1; that is, as the free-floating tip controls deflected 1° the jet vane deflected 3° in the opposite direction. The jet vanes were made of SAE 1020 steel and were identical to the vanes described in reference 13 except for the counterweights attached to the trailing edge of the vane shield to mass balance the fin-vane system. As can be seen in the photograph of the model tail (fig. 21(c)), all four fin-vane assemblies operated independently of each other and therefore provided a limited amount of roll control.

The model was instrumented in order to measure angle of attack, angle of sideslip, jet-vane deflection for one vane in each plane, normal and angular accelerations in both pitch and yaw, Mach number, and rocket chamber pressure. The angle of attack, the angle of sideslip, and the corresponding jet-vane deflections measured for both power-on and power-off conditions are presented in figure 22 and give some insight into the operation of the system. Mach number and dynamic pressure are also presented in figure 22 for reference. The fuselage was extremely elastic because of the high fineness ratio of the model and the lack of stiffness in the case of the Deacon booster rocket. Tracking photography indicated that the body flexed in a number of different modes during the beginning of the flight; but because there was no way to determine the exact amount, the resulting data became qualitative instead of quantitative.

Angle of attack and angle of sideslip have been corrected to the model center of gravity for pitching and yawing velocities; and since the jet vane deflections, δ_α and δ_β, are direct functions of α and β, they were also corrected for the angular velocities in pitch and yaw. Trim conditions of the model without power, obtained during the coasting period of the flight, are also shown in figure 22 at Mach numbers equivalent to those of the power-on data. The values shown for trim conditions for δ_α and δ_β indicate the deflection of the immersed jet vane as the model is trimmed at the corresponding values of α and β, or three times the deflection of the free-floating tip control when influenced by both out-of-trim condition and wash from the forward surfaces. At $M = 1.2$ for example, for power-off, as the model trimmed at $\alpha = -1°$, δ_α was $-7°$ and indicated that the free-floating tip control was deflected $-2.3°$ or that the average angle of the flow at the tip control was increased by approximately 1.3° over the angle of attack. It must be remembered that only a trend in upwash is shown, since the magnitude of the elasticity of the fuselage could not be determined; however,

in some cases upwash from the wings was large enough to cause the model to trim at angles other than the power-off values by actuating the jet vanes through the tip control. This effect was apparent in the pitch oscillations because the model trimmed at larger negative angles of attack for power on than for power off and gave a good indication of the ability of the jet vanes to control the model at angles other than trim. When the wash from the wings became small, as noted by the power-off trim of δ_β near the flight time of 1.2 seconds, the jet-vane system stabilized the model to $\beta = 0^\circ$ although there was an apparent out-of-trim condition of $\beta = -1/2^\circ$.

It can be concluded that the immersed jet vanes were operative in a flight model and produced sufficient force to change the trim of the model; but when these vanes were used with a free-floating tip control, the wash on the control from the forward lifting surfaces contributed to the deflection of the jet vanes sufficient to trim the model at angles other than 0°. The use of this system as a booster is warranted only if appreciable savings in fixed fin area can be obtained and reliable estimates of the flow angularity over the free-floating fin are available.

CONCLUSIONS

From the flight-test results of three delta-wing models having fuselages of square cross section and employing body flap controls, the static test and wind-tunnel tests of body spoilers, the flight test of a fin-actuated jet-vane booster, and various comparisons of control effectiveness the following conclusions may be made:

1. The aerodynamic flap appreciably increases the trim normal-force coefficient throughout the test Mach number range; and during power off, when used in unison with the jet flap, the resulting cambered-body effect produces a further increase in trim of 25 to 50 percent. For similar conditions but with the rocket power on, the trim normal-force coefficient increases from $\frac{1}{3}$ to $2\frac{1}{2}$ times the trim obtained by the aerodynamic flap alone.

2. Comparisons show that estimated values of trim angle of attack and normal-force coefficient for power-on conditions, as obtained from power-off flight data and rocket-static-test data, are less than the measured values. Further comparisons indicate that body flaps require from 2 to $4\frac{1}{2}$ times more deflection than full-span, trailing-edge controls to produce the same trim at similar conditions.

3. The trim drag coefficient for a model equipped with body-flap controls was 30 to 70 percent larger than a corresponding model with tip controls and a round boattailed body.

4. The lift-curve slope of 0.04 to 0.05 per degree for the bodies having a square cross section agreed with that of a corresponding model with tip controls and a boattailed body of circular cross section, but the total movement of the aerodynamic center was twice that of the reference model over the test range of Mach number of 0.7 to 1.7.

5. Although the damping in pitch was low, as is usual for tailless missiles, the damping-in-pitch derivative of the body having a square cross section was consistently greater than that of a model with similar wings but with a boattailed body of circular cross section.

6. Wind-tunnel tests conducted at a Mach number of 1.62 show that aerodynamic spoilers mounted on a body of square cross section are 25 to 45 percent more effective than when mounted on a body of circular cross section, and the effective location of the control center of pressure remains almost constant with angle of attack and control height except for the large spoiler on the body of circular cross section. Changing the body cross section from circular to square increases the slope of the normal-force coefficient by 30 percent. Control effectiveness was found to be nonlinear with angle of attack.

7. Rocket static tests established that a jet spoiler tilts the thrust axis nearly linearly with the amount of nozzle exit area blocked by the spoiler. In order to deflect the thrust vector 5°, a 4-percent penalty in thrust impulse must be taken; this impulse loss, or spoiler drag, was doubled when the spoiler was seperated from the nozzle by a relatively large gap of 6 percent of the exit diameter.

8. In a comparison of aerodynamic spoilers with aerodynamic flaps, both mounted at the base of a body of square cross section, it appears that spoilers are as effective as flaps and can be operated without the large hinge moments associated with flaps.

9. For reaction controls with a 2-percent loss in thrust impulse, the immersed jet vane, the jet flap, and the jet spoiler deflect the thrust vector 1°, 3°, and $4\frac{1}{2}^\circ$, respectively.

10. Qualitative results from a flight test of a fin-actuated jet-vane booster indicated that the trim of a model booster combination can be changed with immersed jet vanes but that the wash from the forward surfaces, the wings of the model, influenced the floating angle of the tip control which actuated the jet vanes. The use of this system of

stabilization is warranted only if appreciable savings in fixed fin area can be obtained and if reliable estimates of the flow angularity over the free-floating fin are available.

Langley Aeronautical Laboratory,
National Advisory Committee for Aeronautics,
Langley Field, Va., December 3, 1956.

REFERENCES

1. Friedman, Henry: Summary Report of A-4 Control and Stability. Summary Rep. F-SU-2152-ND, Air Materiel Command, U. S. Army Air Forces, June 1947.

2. Eisenklam, P., and Rowe, P.: Supersonic Jet Deflection. Part II. Deflection by Inclined Tubular Extensions. PDGW Rep./EMR/52/5 (Imperial College Rep. JRL 25), British Ministry of Supply, Sept. 1952.

3. Powell, W. B.: Experimental Investigations With Jet Control Vanes. Progress Rep. No. 4-30 Jet Propulsion Lab., C.I.T., 1948.

4. Rosan, H. J.: LTV-N-4b1 (VTV-1) Design, Development and Flight Test. CAL/CM-547, CAL-1-D-2, Cornell Aero. Lab., May 27, 1949.

5. Rosen, Milton W., Bridger, James M., and Jones, Alton E.: Rocket Research Report No. X - The Viking 7 Firings. Rep. No. 3946, Naval Res. Lab., Radio Div. I, Mar. 25, 1952.

6. Main, J. H., and Winer, R.: Studies of Jet Vanes in Rockets - III. Progress Rep. ABL/R-29, (Contract NOrd 10431), Hercules Powder Co., Allegany Ballistics Lab. (Cumberland, Md.) Jan. 1950.

7. Lein, H. S.: Jet Vane Controlled Bomber Defense Missile. Contract No. AF-33(038)-22346, MX-1601, Cornell Aero. Lab., Inc. Rep. No. BE-753-S-7, Quarterly Progress Rep. No. 5, Apr. - June 1952.

8. Fiedler, W. A.: Wide Angle Jetevator - Configuration "A" (Project TED MTC SI-502). Memo. Rep. No. 2-54, Component Test Dept., U. S. Naval Air Missile Test Center (Pt. Mugu, Calif.), Jan. 20, 1954.

9. Alexander, Sidney R.: An Extension of a Fighter-to-Fighter Missile Design Study. NAVAER DR Rep. 1580, Bur. Aero., Mar. 1954.

10. Anon: Report on Engineering Study and Investigation of the Problems of Jet-Thrust Systems As Related to Directional Control of an Airplane. Rep. No. 3817-5 (Supplement to Rep. No. 3817-3), Ryan Aero. Co., Feb. 11, 1948.

11. Bond, Aleck C.: An Experimental Investigation of a Flat-Plate Paddle Jet Vane Operating on a Rocket Jet. NACA RM L50I20, 1950.

12. Wineman, Andrew R.: Preliminary Investigation of a Fin-Actuated Jet-Vane Control System for Stabilization of Rocket-Powered Models. NACA RM L50K17, 1951.

13. Giladett, Leo V., and Wineman, Andrew R.: Investigation of Vanes Immersed in the Jet of a Solid-Fuel Rocket Motor. NACA RM L52F12, 1952.

14. Carlson, Harry W., and Gapcynski, John P.: An Experimental Investigation at a Mach Number of 2.01 of the Effects of Body Cross-Section Shape on the Aerodynamic Characteristics of Bodies and Wing-Body Combinations. NACA RM L55E23, 1955.

15. Gillis, Clarence L., Peck, Robert F., and Vitale, A. James: Preliminary Results From a Free-Flight Investigation at Transonic and Supersonic Speeds of the Longitudinal Stability and Control Characteristics of an Airplane Configuration With a Thin Straight Wing of Aspect Ratio 3. NACA RM L9K25a, 1950.

16. Scarborough, James B.: Numerical Mathematical Analysis. Second ed., The Johns Hopkins Press (Baltimore), 1950.

17. Boyd, John W. and Pfyl, Frank A.: Experimental Investigation of Aerodynamically Balanced Trailing-Edge Control Surfaces on an Aspect Ratio 2 Triangular Wing at Subsonic and Supersonic Speeds. NACA RM A52L04, 1953.

18. Moul, Martin T., and Baber, Hal T., Jr.: The Longitudinal Stability and Control Characteristics of a 60° Delta-Wing Missile Having Half-Delta Tip Controls As Obtained From a Free-Flight Investigation at Transonic and Supersonic Speeds. NACA RM L52H14, 1952.

19. Gillis, Clarence L., and Chapman, Rowe, Jr.: Summary of Pitch-Damping Derivatives of Complete Airplane and Missile Configurations as Measured in Flight at Transonic and Supersonic Speeds. NACA RM L52K20, 1953.

TABLE I

MASS CHARACTERISTICS OF MODELS 1, 2, AND 3

Model 1	
First coast	
Weight, lb	118.0
Center of gravity, station, in.	50.15
Moment of inertia, I_Y, slug-ft^2	7.53
Second coast	
Weight, lb	92.0
Center of gravity, station, in.	49.56
Moment of inertia, I_Y, slug-ft^2	6.92
Model 2	
First coast	
Weight, lb	123.8
Center of gravity, station, in.	50.38
Moment of inertia, I_Y, slug-ft^2	7.97
Second coast	
Weight, lb	95.6
Center of gravity, station, in.	49.63
Moment of inertia, I_Y, slug-ft^2	7.36
Model 3	
First coast	
Weight, lb	124.0
Center of gravity, station, in.	50.22
Moment of inertia, I_Y, slug-ft^2	8.71
Second coast	
Weight, lb	98.0
Center of gravity, station, in.	49.32
Moment of inertia, I_Y, slug-ft^2	8.10

TABLE II

ACCURACY OF DATA

[All errors are plus or minus]

Calculated Probable Errors for Models 1, 2, and 3						
	M = 0.75		M = 1.10		M = 1.58	
	First coast	Second coast	First coast	Second coast	First coast	Second coast
M	0.018	0.051	0.008	0.015	0.005	0.009
$C_{N_{trim}}$	0.0059	0.0406	0.0022	0.0268	0.0015	0.0103
C_p	0.059	0.113	0.034	0.051	0.010	0.023
C_A	0.0013		0.0021	0.0025	0.0006	0.0015
C_L	0.0059		0.0042		0.0026	
C_D	0.0165		0.0026		0.0060	
α_{trim}, deg	0.2		0.2		0.2	
C_{L_α}	0.0029		0.0076		0.0034	
$\frac{100x_{ac}}{\bar{c}}$	1.82		5.25		3.13	
$t_{1/2}$, sec	0.26		0.09		0.04	
$C_{m_q} + C_{m_{\dot{\alpha}}}$	4.80		1.76		4.30	

Estimated Errors in Supplementary Tests					
Static rocket		Langley 9-inch supersonic tunnel		Immersed jet-vane booster	
Lift, lb	6	C_N	0.0085	α and β, deg	0.2
Hinge moment, in-lb	6	C_m	0.0019	δ_α and δ_β, deg	0.6
Thrust, lb	24	α, deg	0.05		

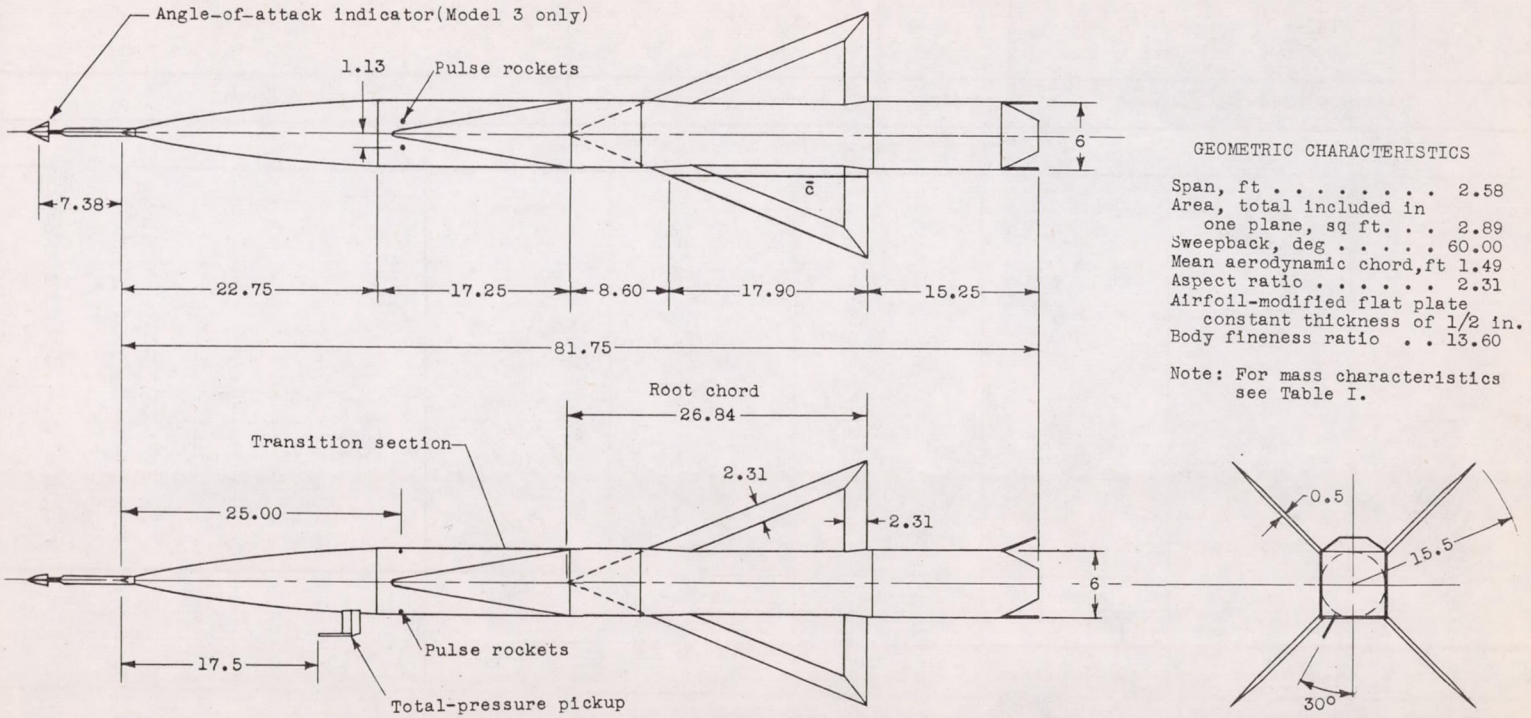

(a) Drawing of the square-bodied paddle-type control model.

Figure 1.- Sketches of flight model showing dimensions and locations of the various components. All dimensions are in inches unless otherwise noted.

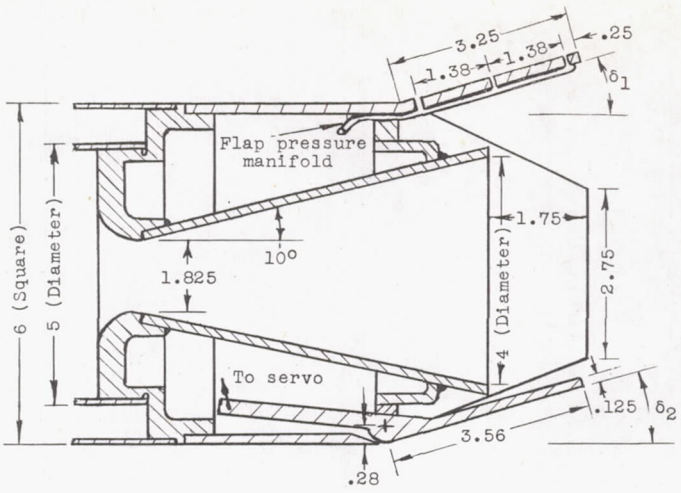

(b) Detailed sketch of modified nozzle and flap assembly.

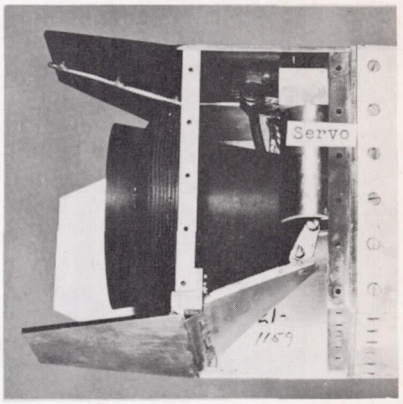

L-81728.1

(c) Photograph of flap assembly. Side and bottom covers removed.

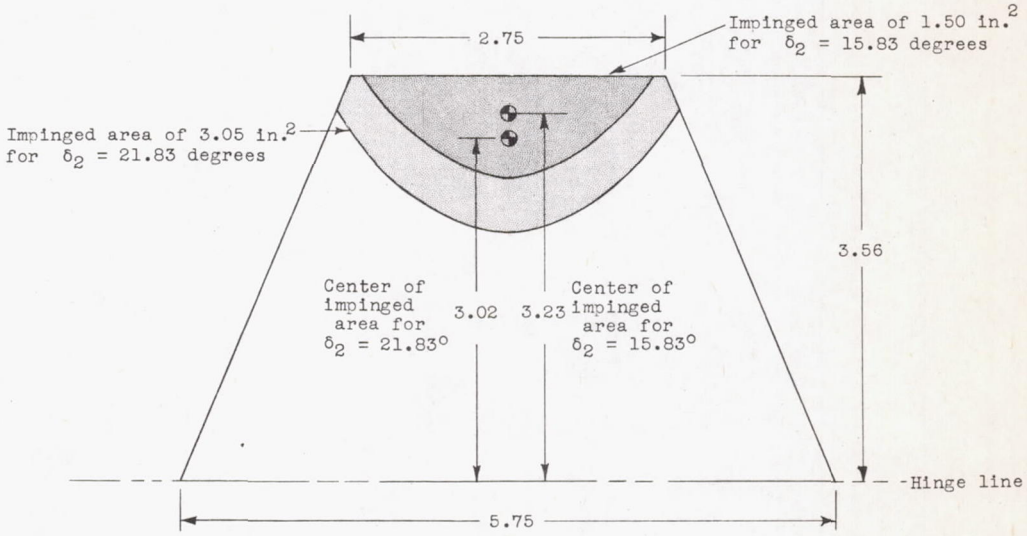

(d) Sketch showing jet-blast impingement on flap and location of centers of impinged area for δ_2 of 15.83° and 21.83°.

Figure 1.- Concluded.

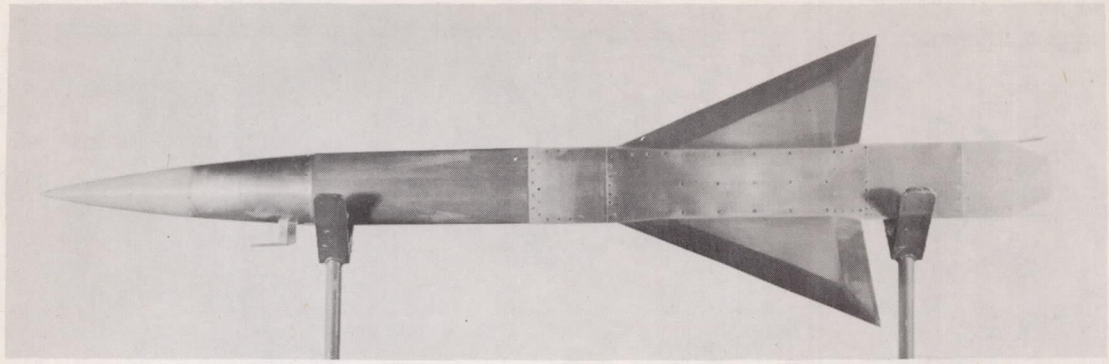

(a) Model 1. Side view.

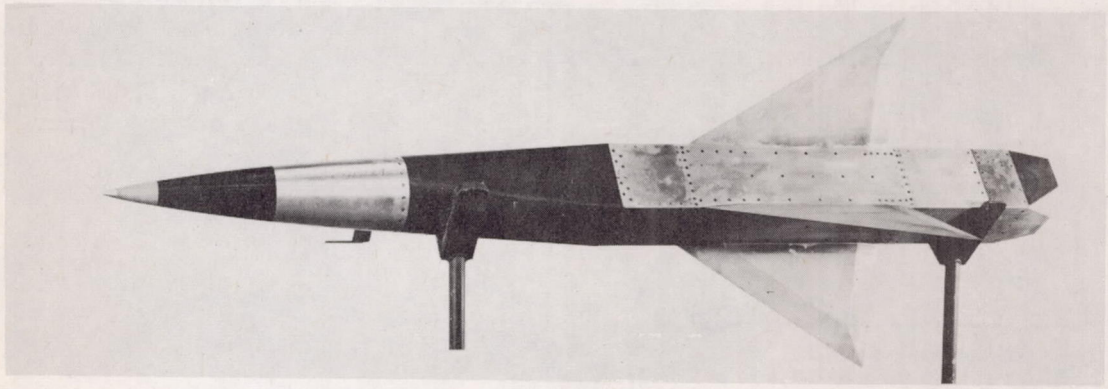

(b) Model 2. Three-quarter front view.

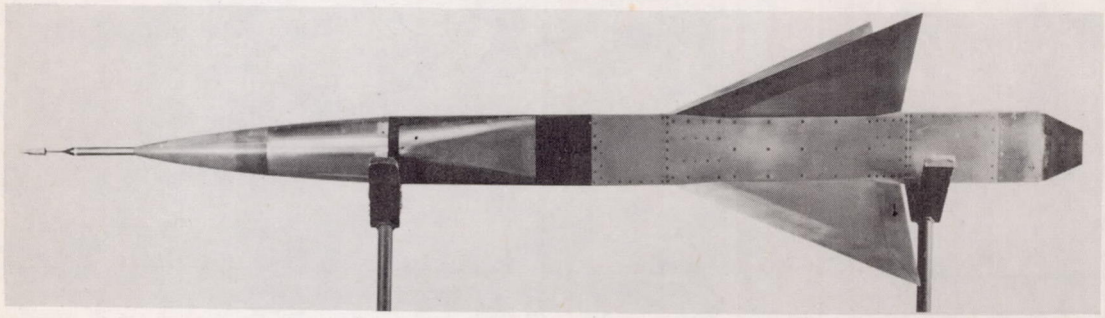

(c) Model 3. Top view. L-95899

Figure 2.- Photographs of flight models.

First coast	Second coast and Power on
Model 1 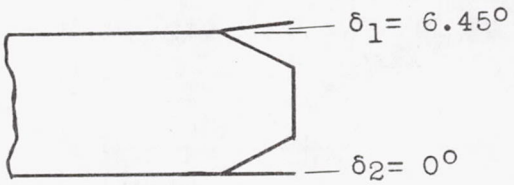	Model 1 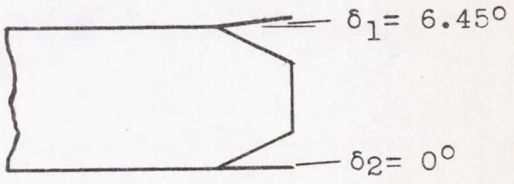
Model 2 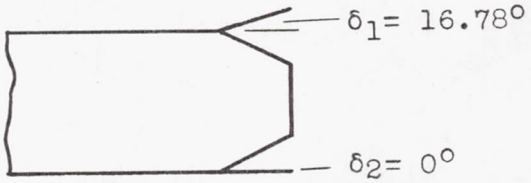	Model 2 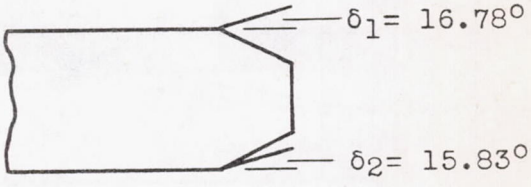
Model 3 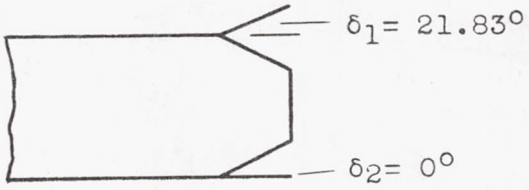	Model 3 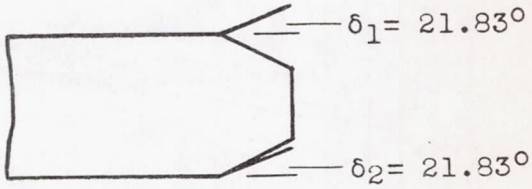

Figure 3.- Body-control settings for flight models.

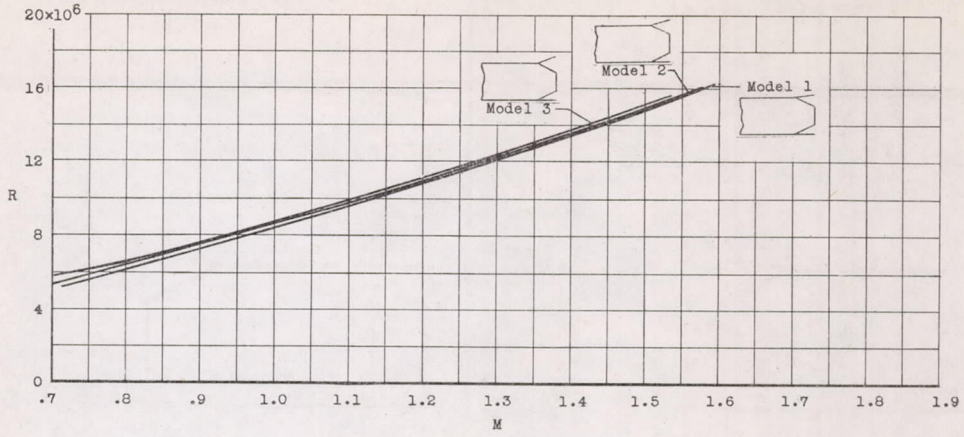

(a) First coast.

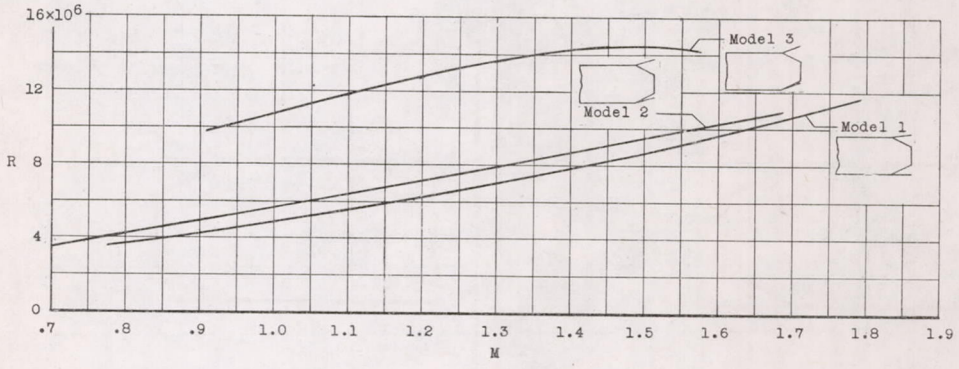

(b) Second coast.

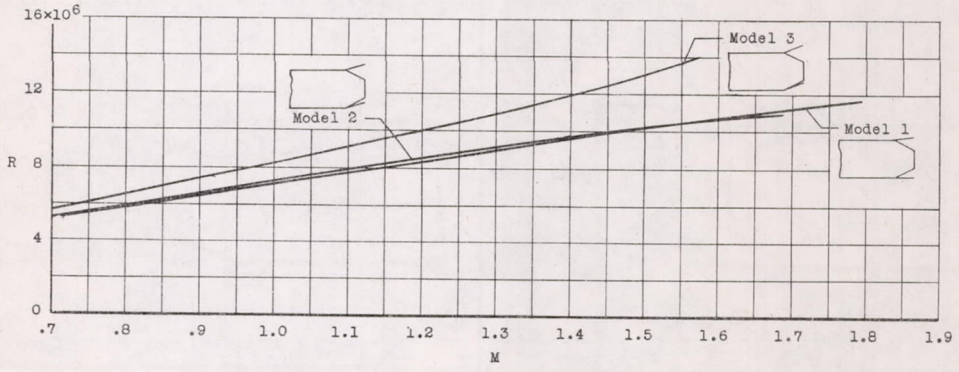

(c) Power on.

Figure 4.- Variation of Reynolds number with Mach number.

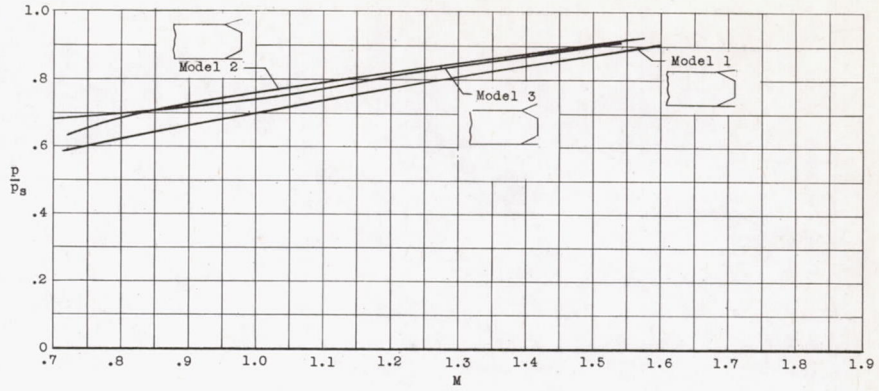

(a) First coast.

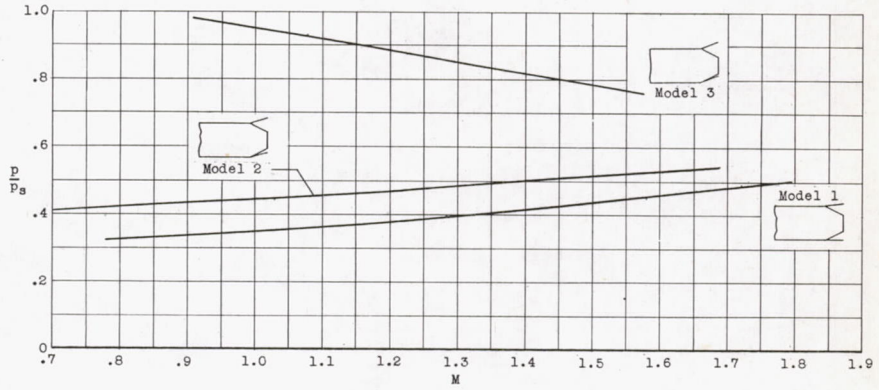

(b) Second coast.

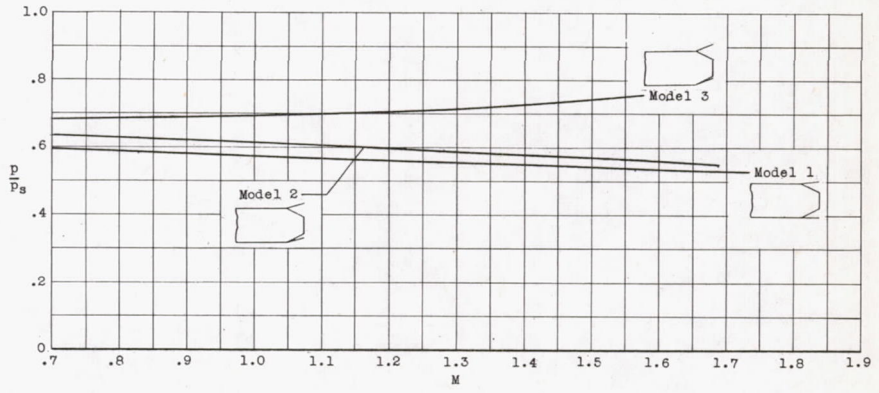

(c) Power on.

Figure 5.- Variation of static pressure ratio with Mach number.

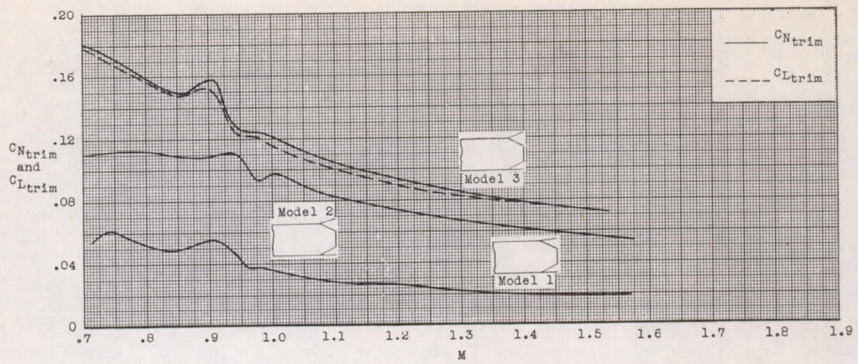

(a) First coast.

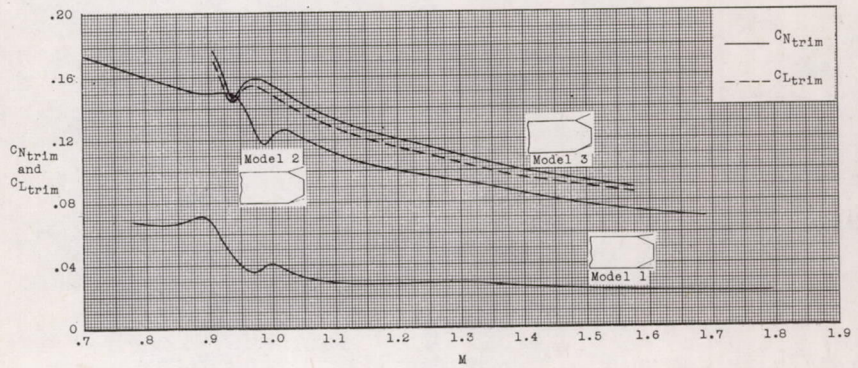

(b) Second coast.

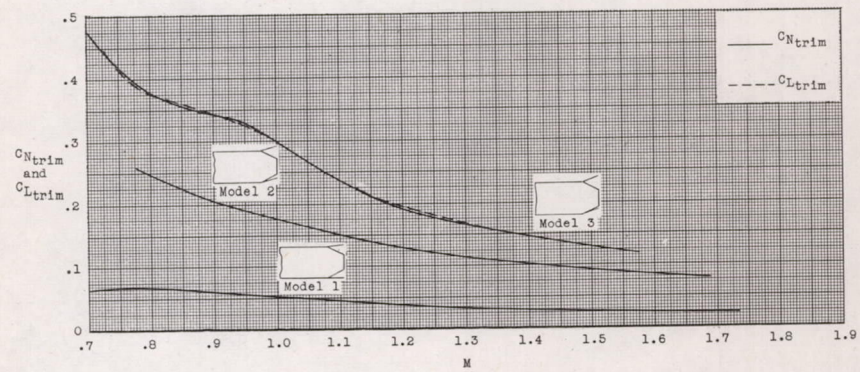

(c) Power on.

Figure 6.- Variation of $C_{N_{trim}}$ and $C_{L_{trim}}$ with Mach number. (Ordinate scale for (c) different from (a) and (b).)

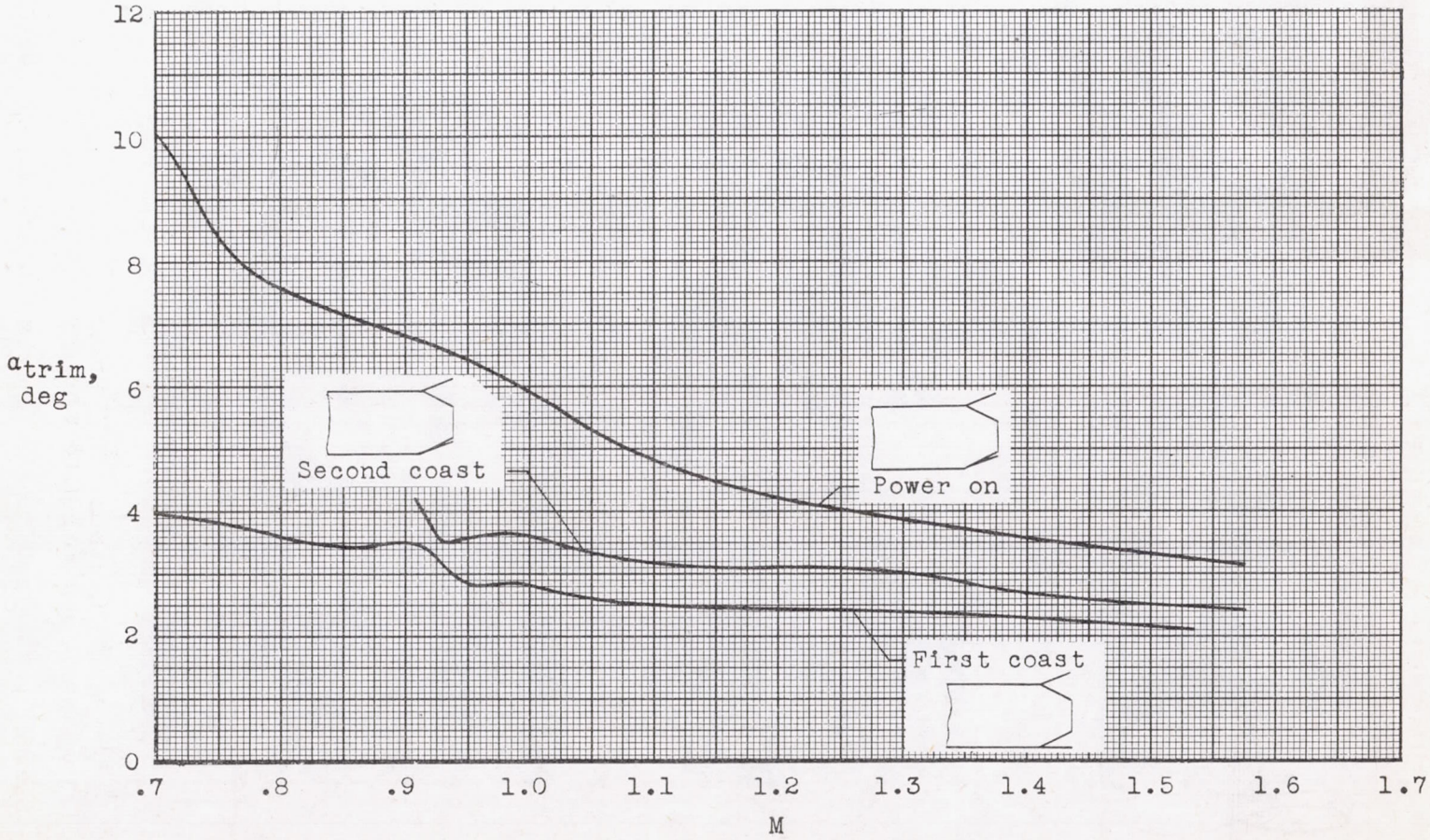

Figure 7.- Variation of trim angle of attack with Mach number for model 3.

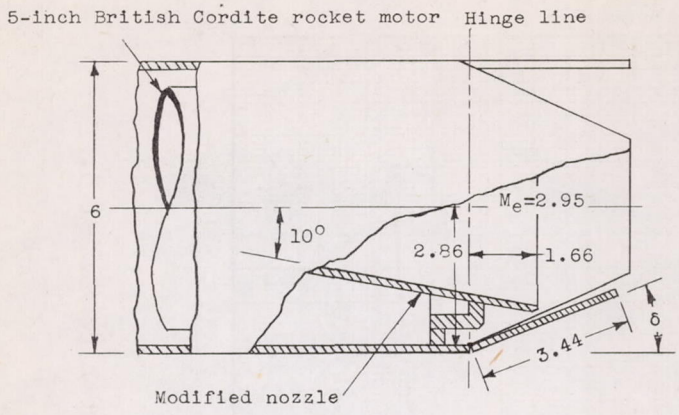

All dimensions are in inches.

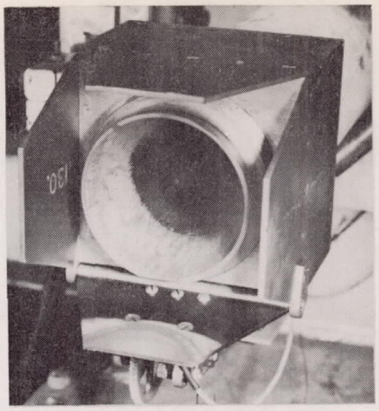

L-81509

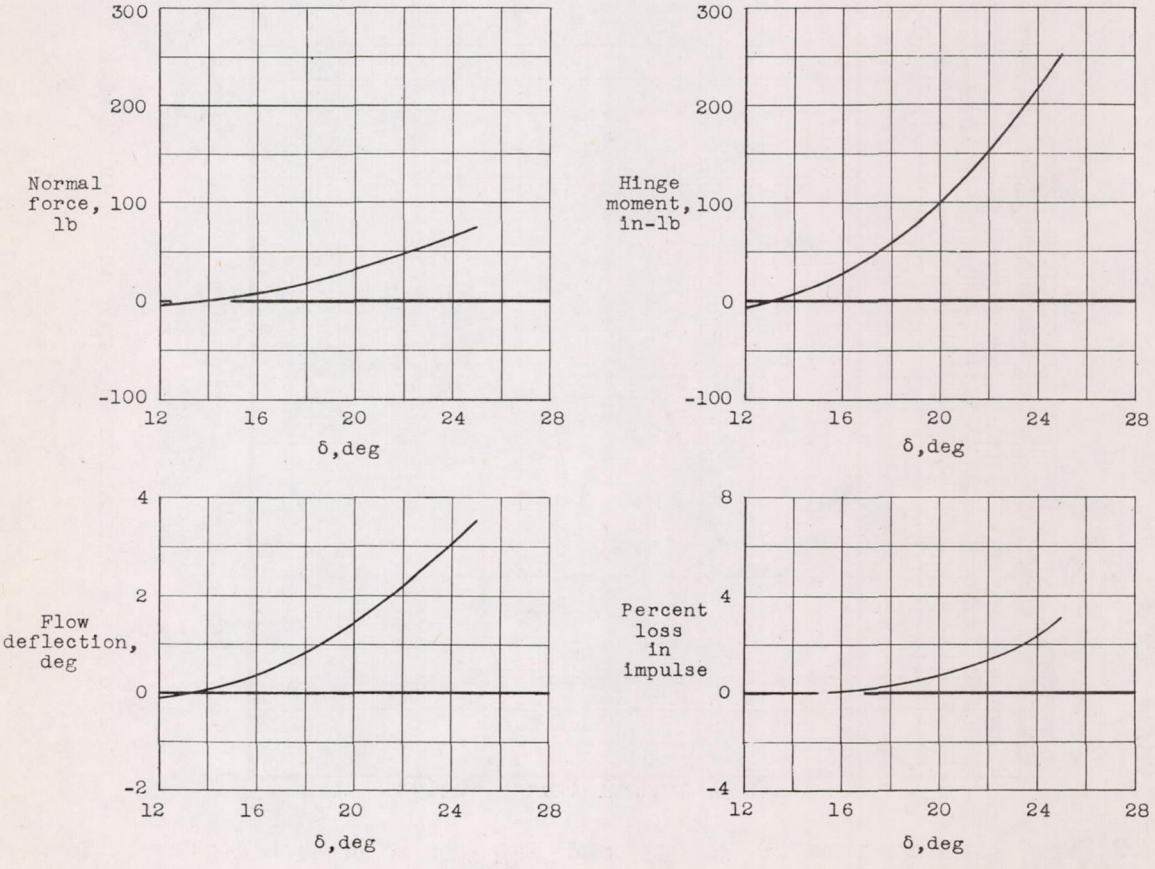

Figure 8.- Sketch, photograph, and data from static test of jet flap.

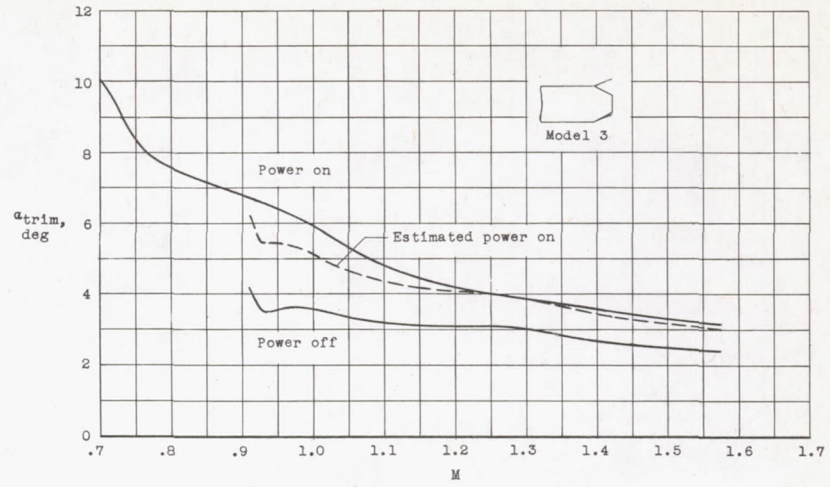

(a) Trim angle of attack.

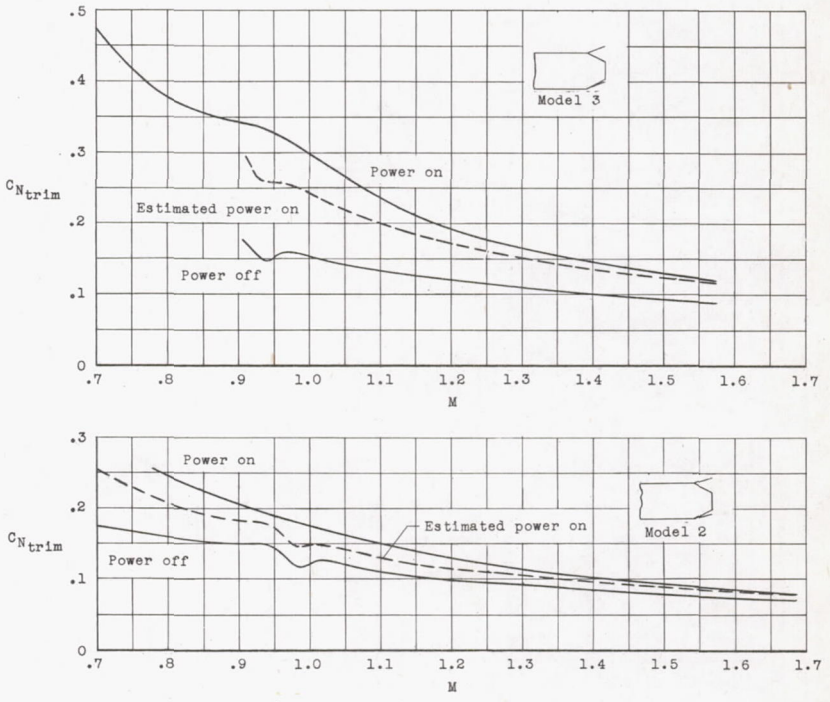

(b) Trim normal-force coefficient.

Figure 9.- Variation of α_{trim} and $C_{N_{trim}}$ with Mach number of actual power-on and power-off flight data compared with estimated power-on data from the static test for flap deflections of 21.83° and 16.78°.

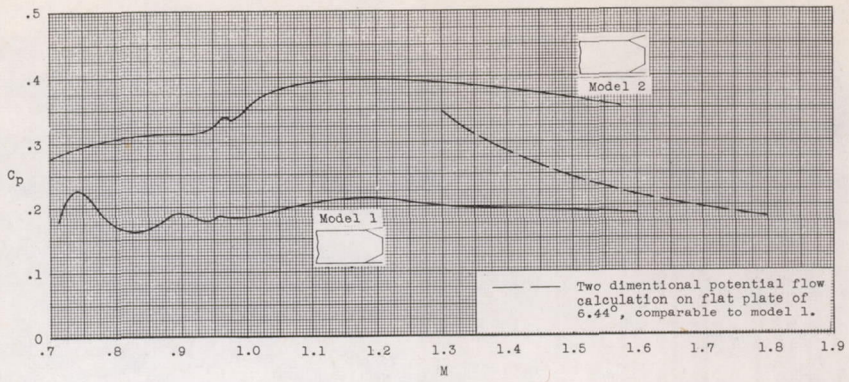

(a) First coast.

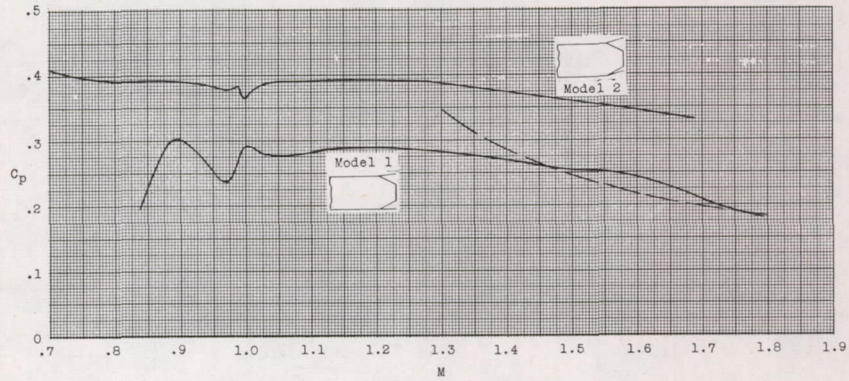

(b) Second coast.

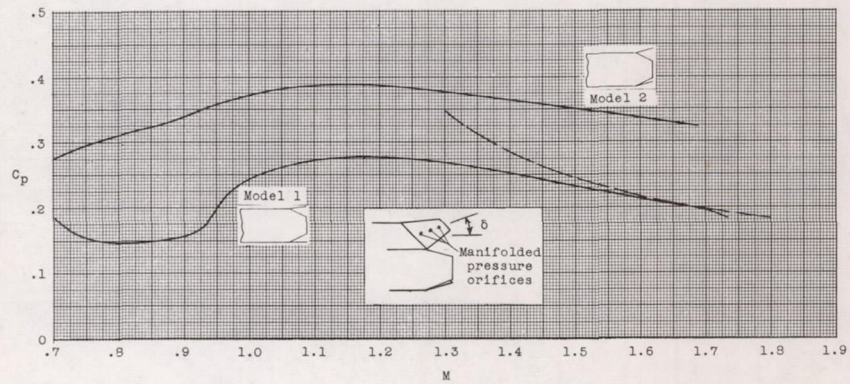

(c) Power on.

Figure 10.- Variation of pressure coefficient with Mach number.

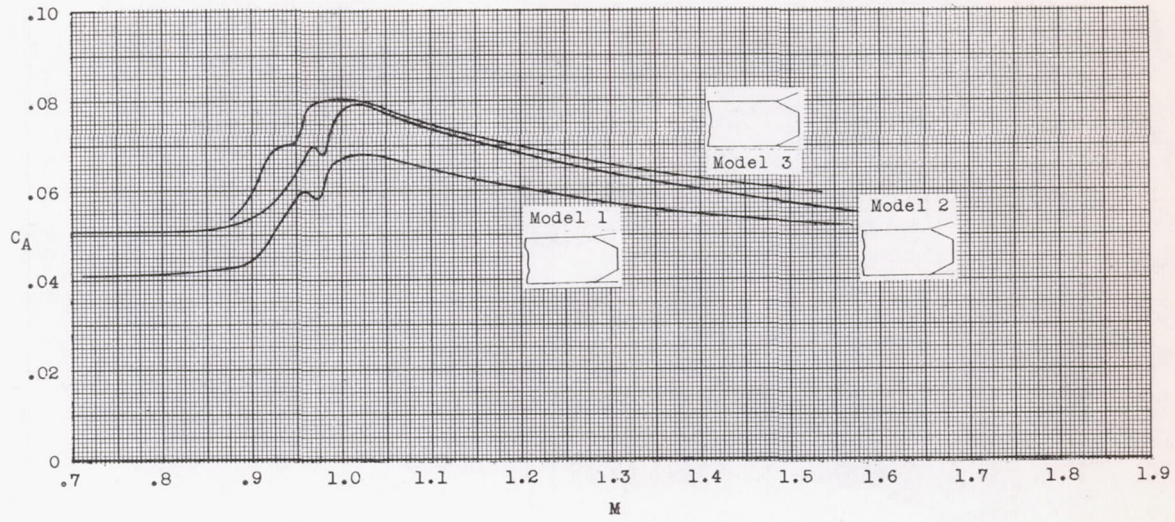

(a) First coast.

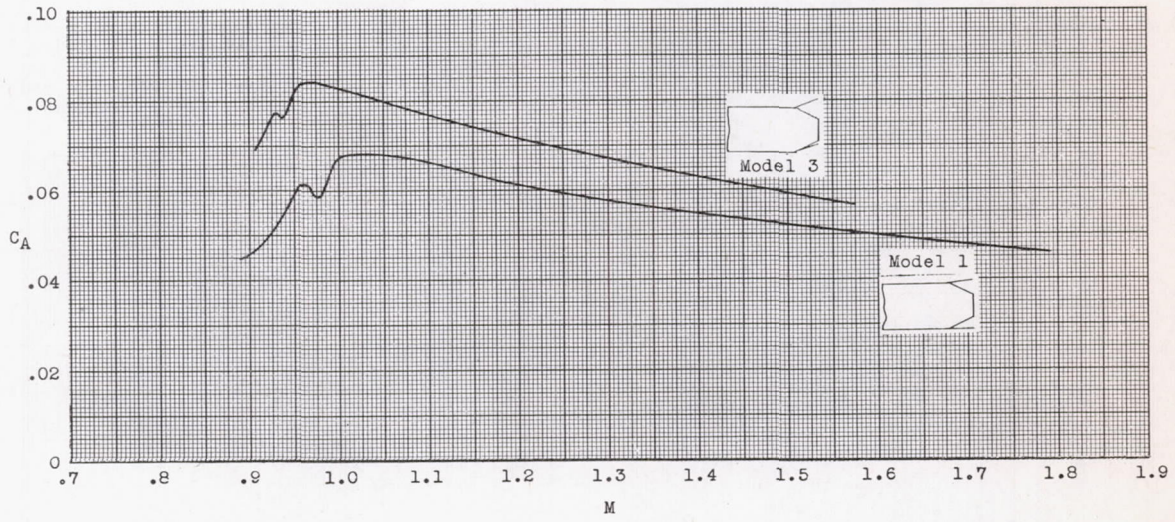

(b) Second coast.

Figure 11.- Variation of axial-force coefficient with Mach number. Coefficients are based on the wing area in one plane.

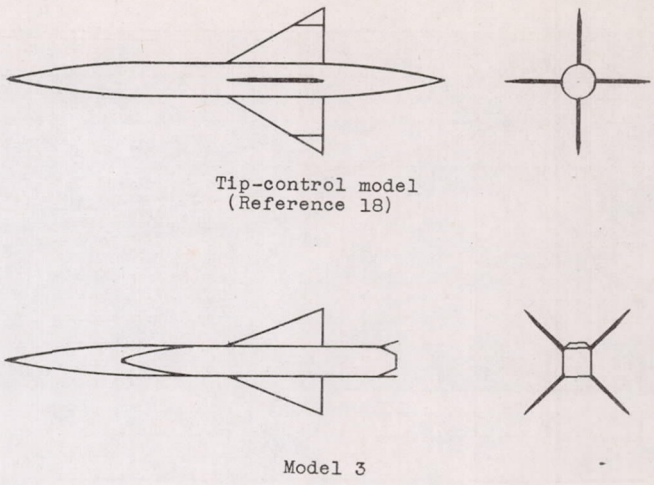

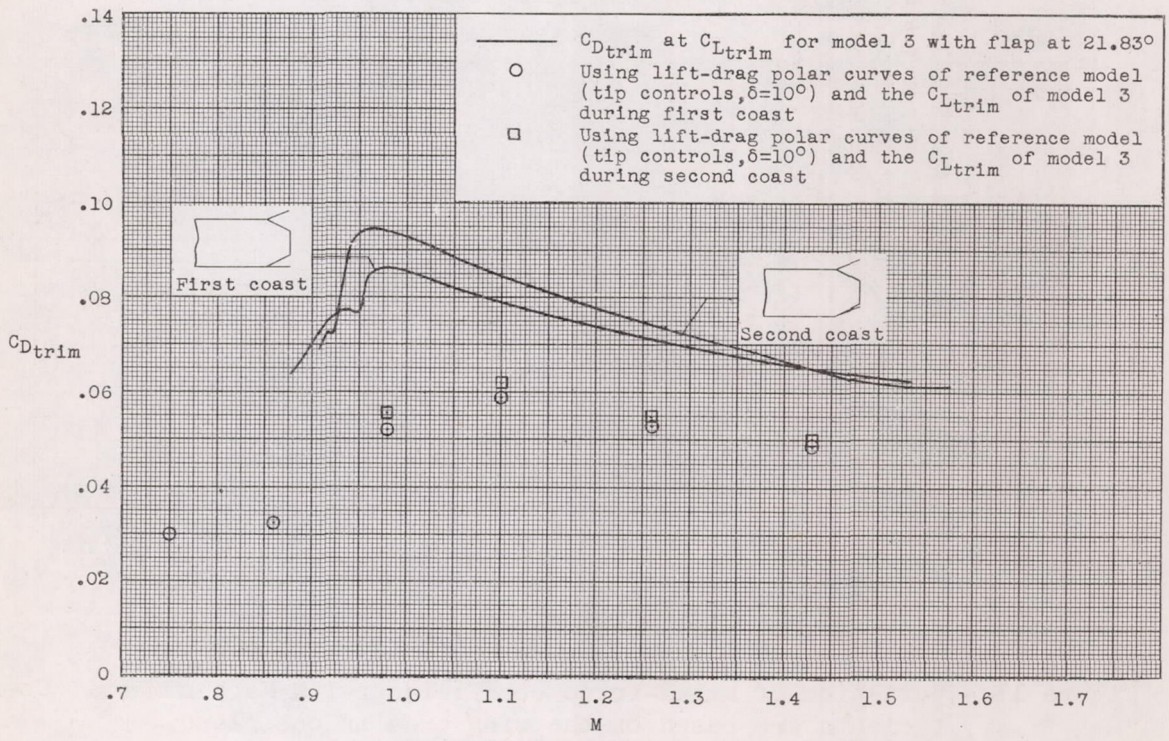

Figure 12.- Comparison of $C_{D_{trim}}$ at $C_{L_{trim}}$ of model 3 with points from polar curves of reference 18.

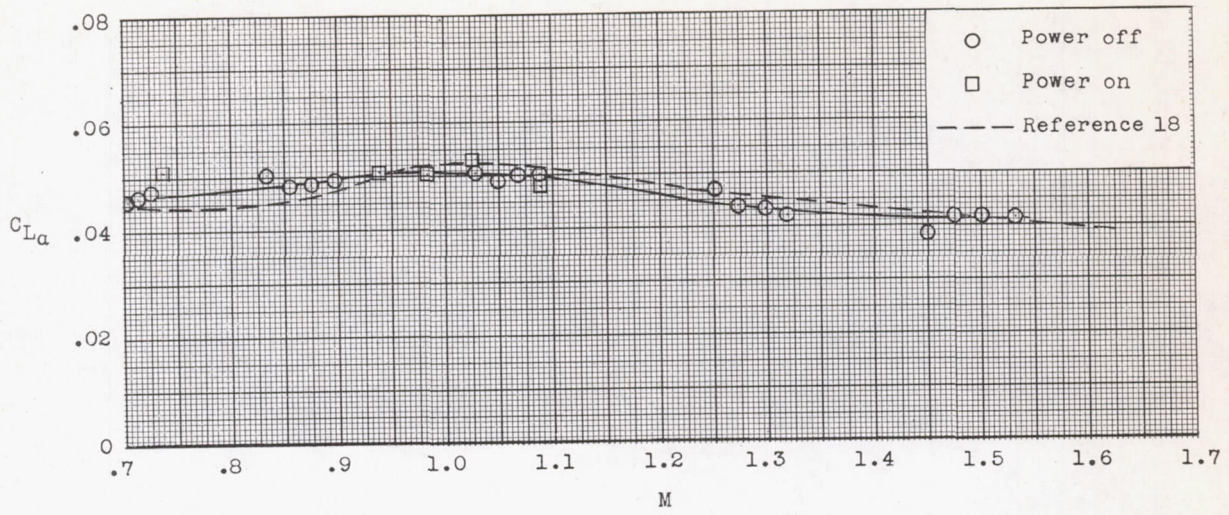

(a) Lift-curve slope.

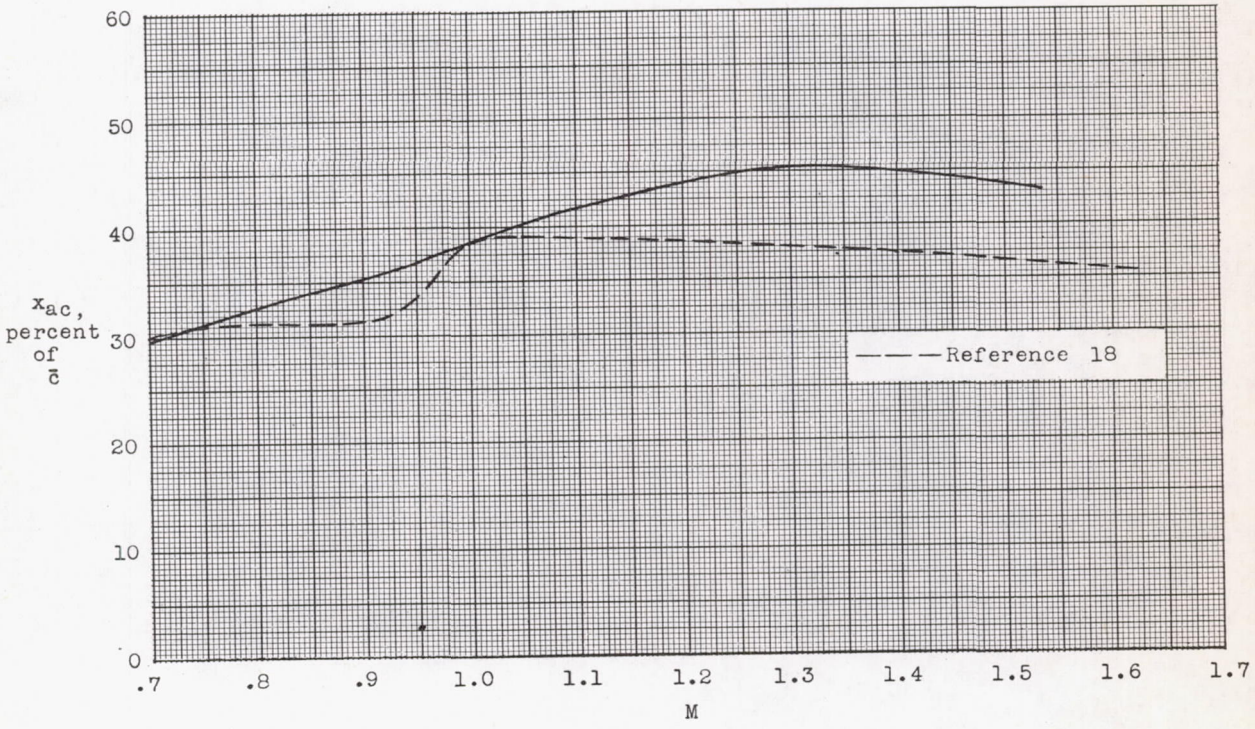

(b) Aerodynamic center.

Figure 13.- Variation of lift-curve slope and location of aerodynamic center with Mach number for model 3; $\delta_1 = 21.83^\circ$.

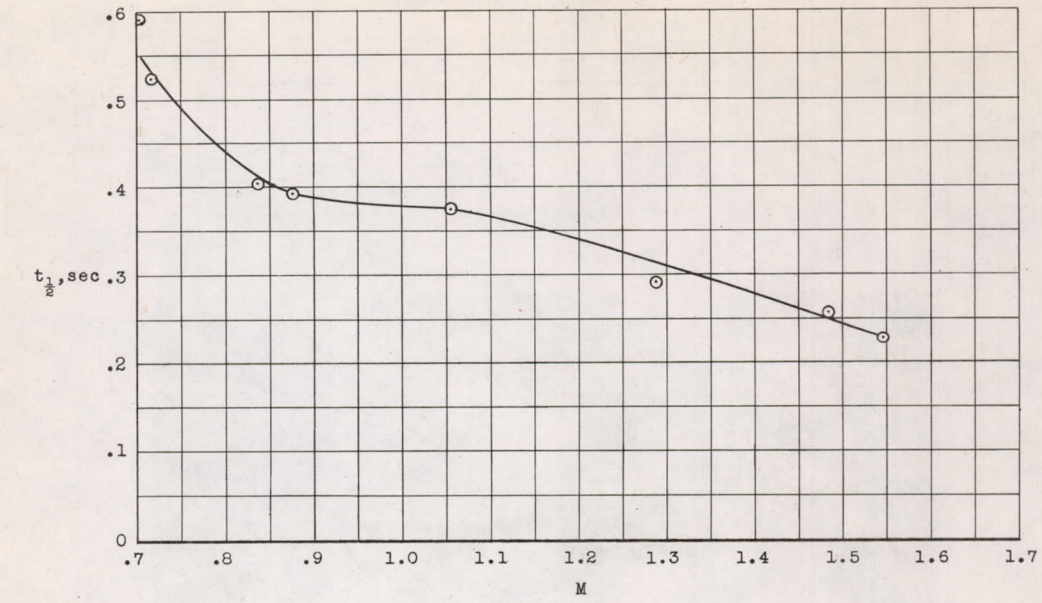

(a) Time to damp to one-half amplitude.

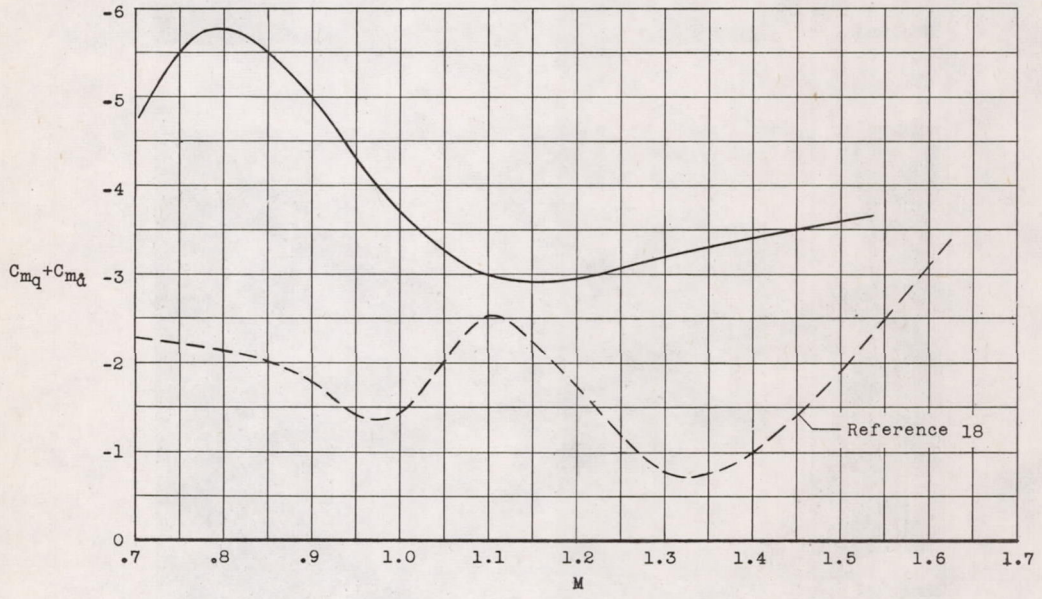

(b) Pitch damping.

Figure 14.- Variation of time to damp to one-half amplitude and damping-in-pitch derivative with Mach number for model 3; $\delta_1 = 21.89^\circ$; center of gravity located $0.09\bar{c}$ behind leading edge of $\bar{c}$.

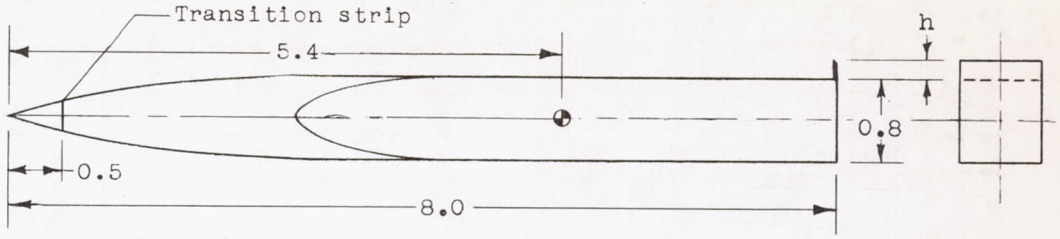

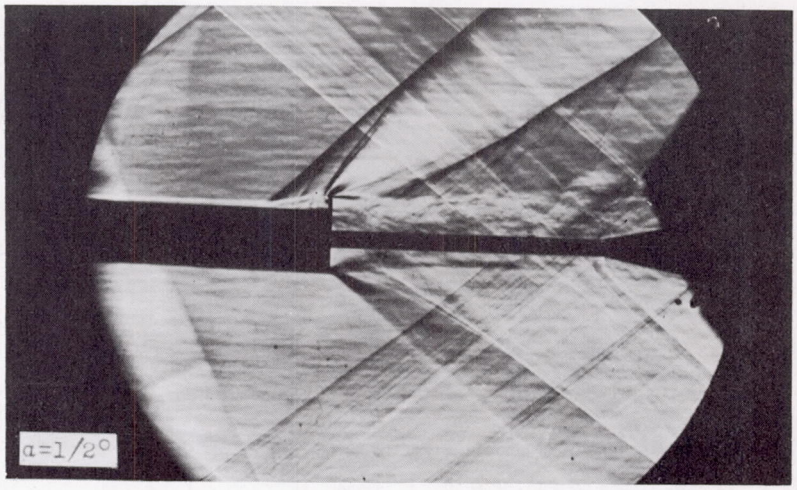

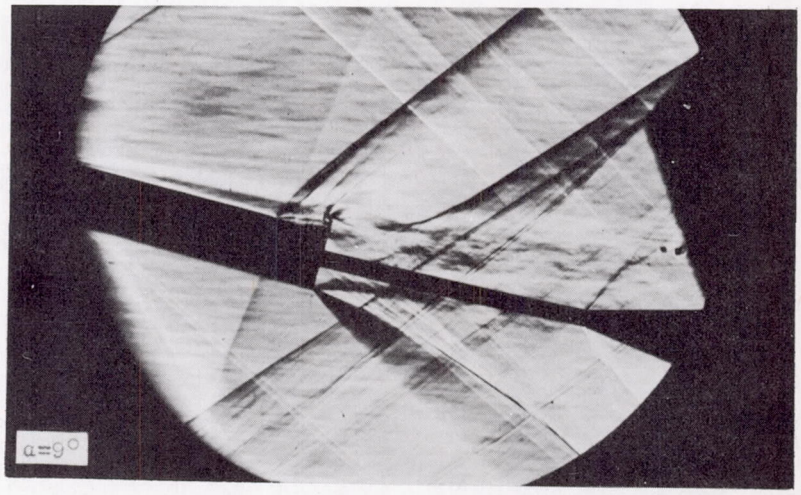

(a) Body having square cross section. L-95900

Figure 15.- Sketch of wind-tunnel models with spoilers and schlieren photographs of models at $\alpha = \frac{1}{2}^{\circ}$ and $\alpha = 9^{\circ}$; $M = 1.62$; $R = 5.7 \times 10^{6}$; $h/d = 0.25$. All dimensions are in inches.

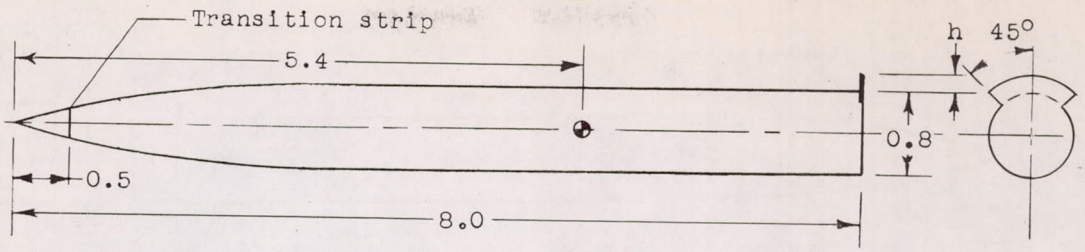

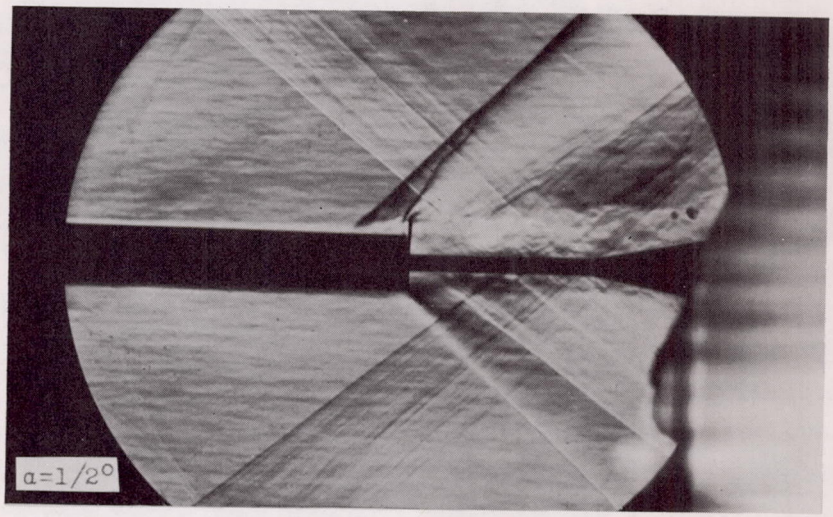

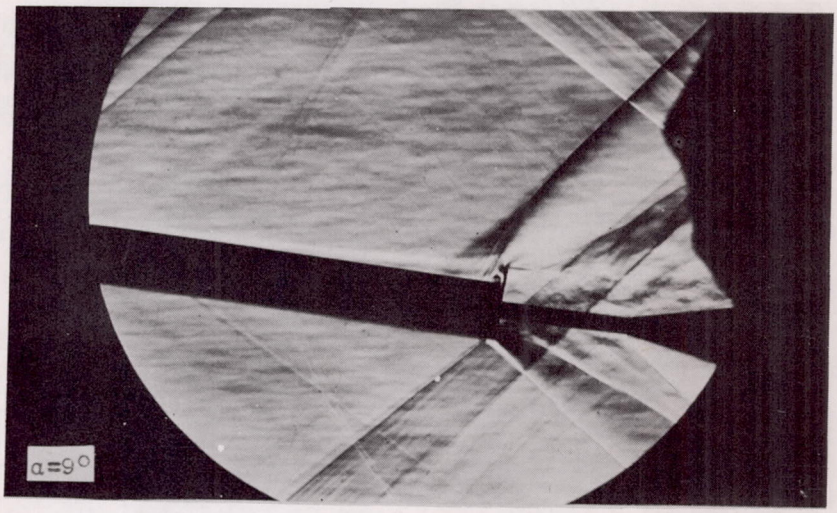

(b) Body having circular cross section. L-95901

Figure 15.- Concluded.

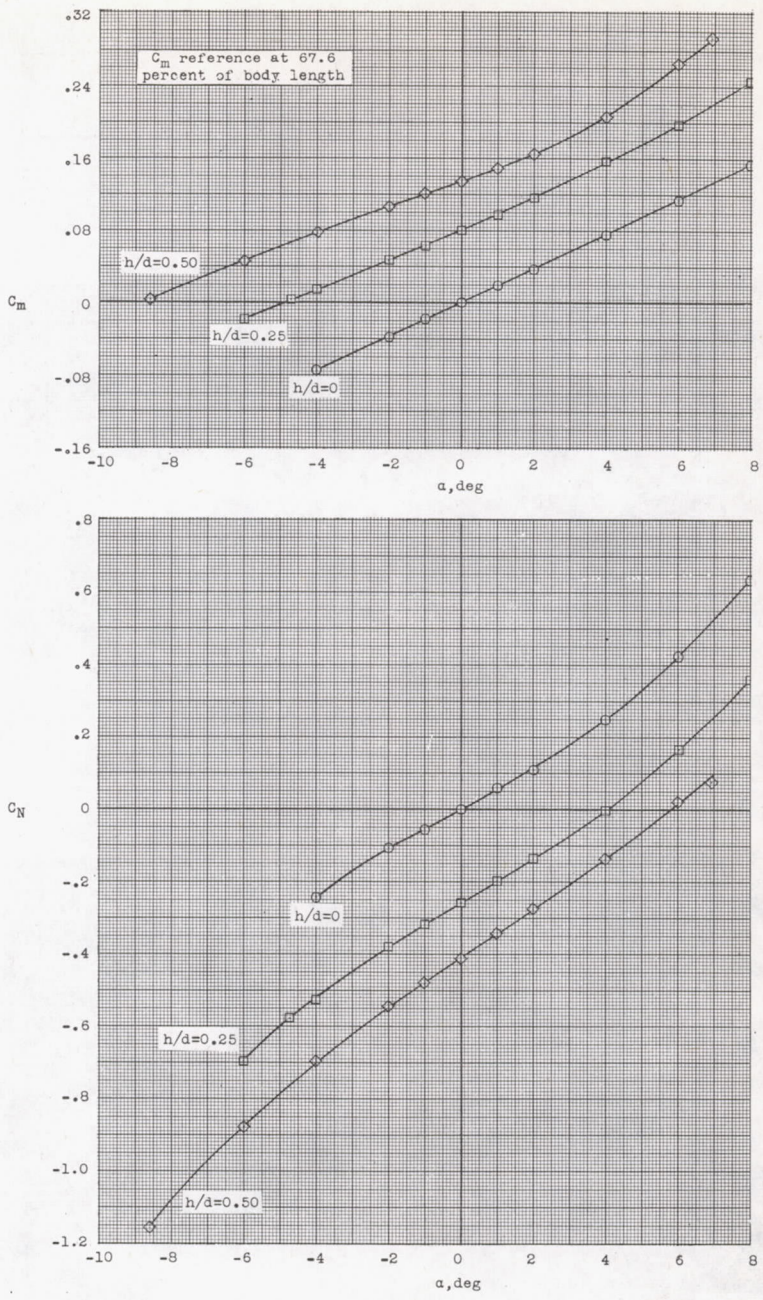

(a) Body with square cross section.

Figure 16.- Variation of C_m and C_N with angle of attack for body spoilers mounted on bodies with square and circular cross section. M = 1.62; coefficients based on body cross-sectional area and body length.

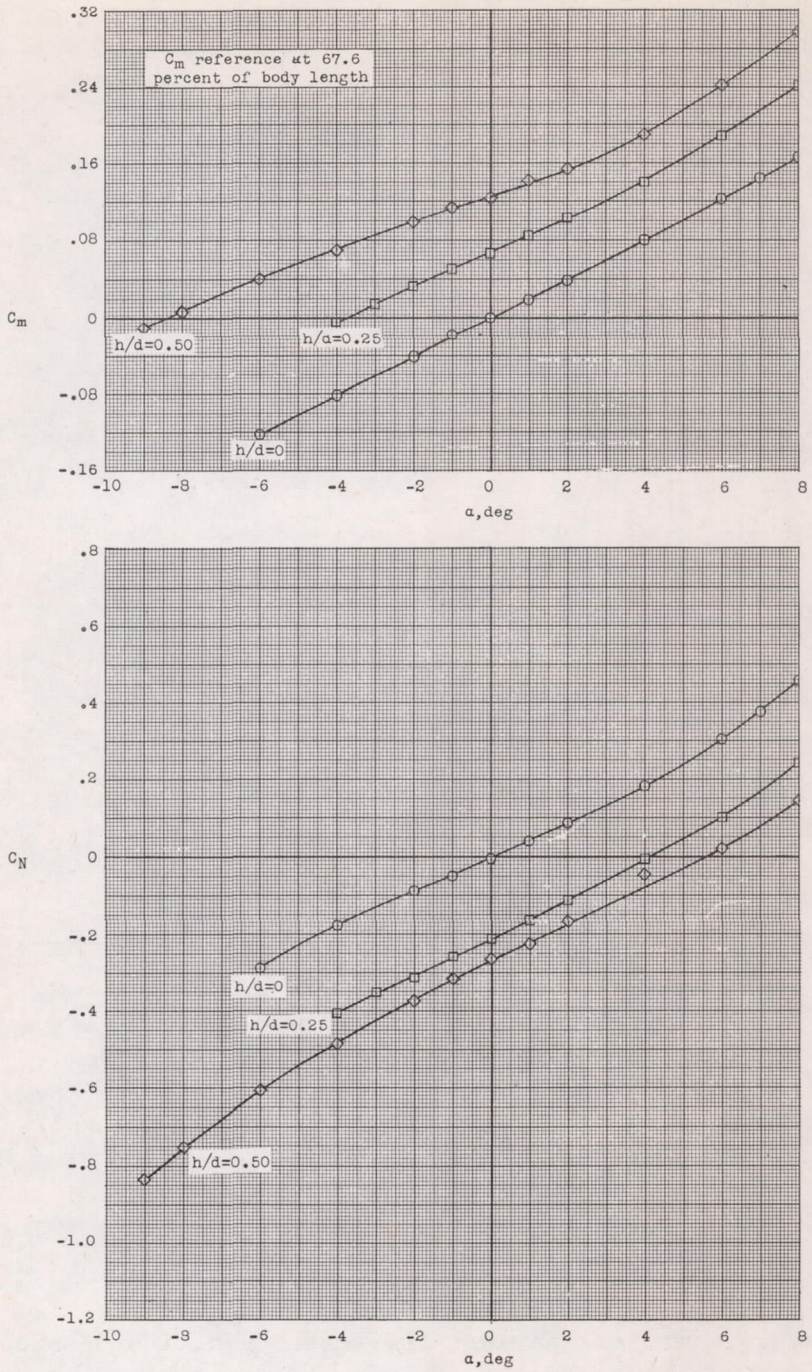

(b) Body with circular cross section.

Figure 16.- Concluded.

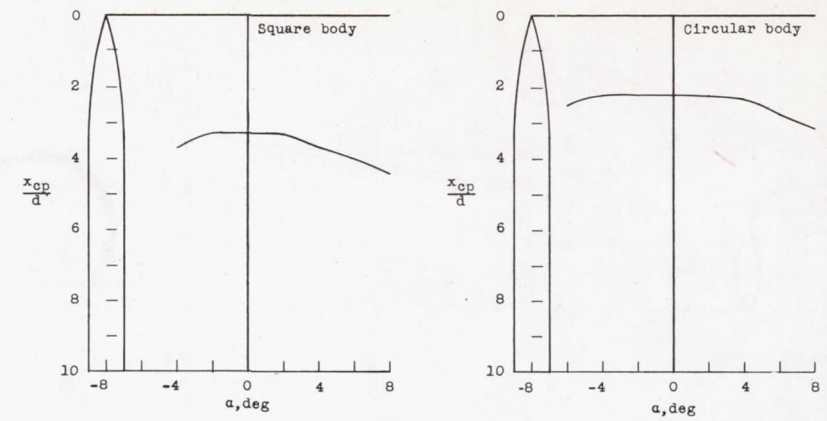

(a) Center of pressure of body alone.

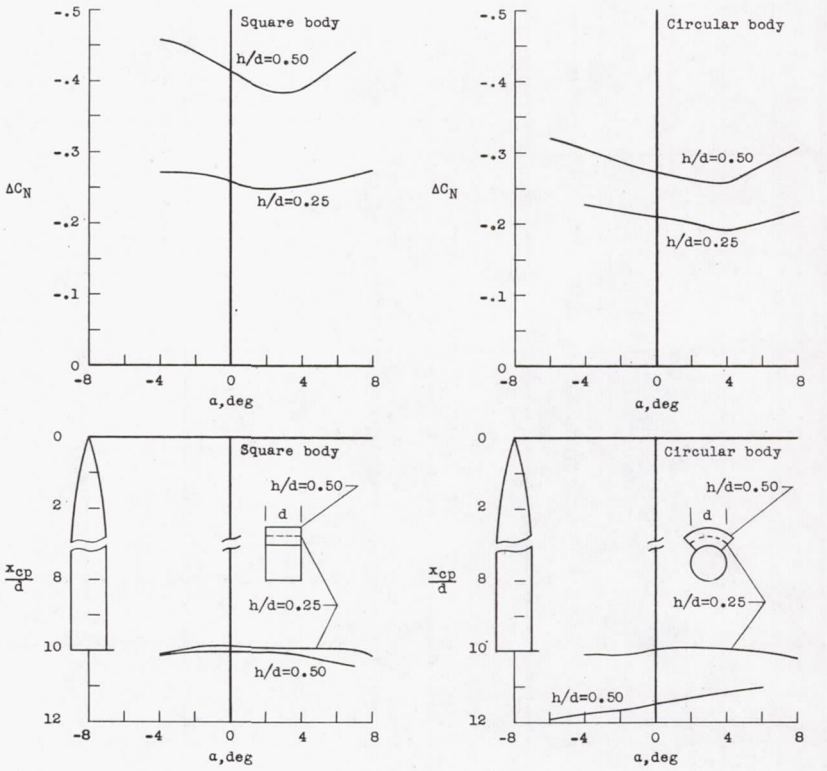

(b) Change in normal coefficient due to the addition of spoiler; also effective center of pressure of spoiler.

Figure 17.- Effectiveness of spoilers on bodies of square and circular cross section; coefficients are based on body cross-sectional area; M = 1.62.

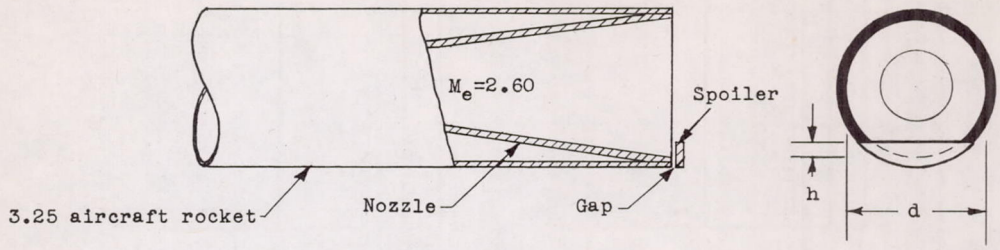

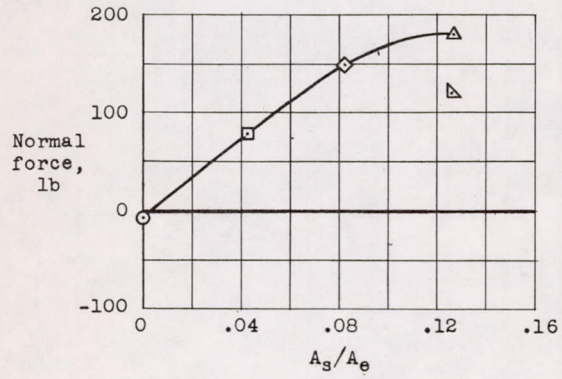

No hinge moment

Symbol	h/d	gap size
○	No spoiler	
□	0.087	None
◇	.136	None
△	.174	None
◺	.174	0.058d

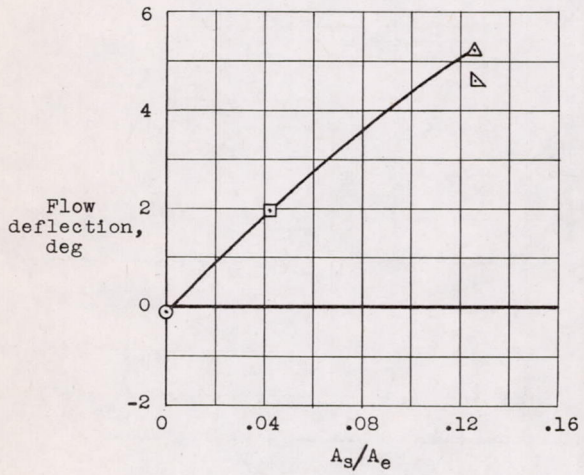

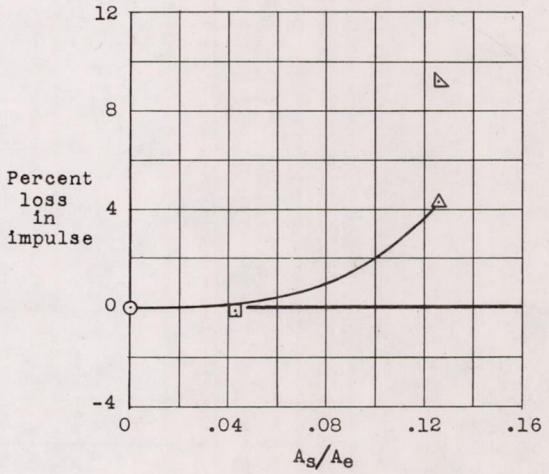

Figure 18.- Sketch and data from static test of jet spoiler.

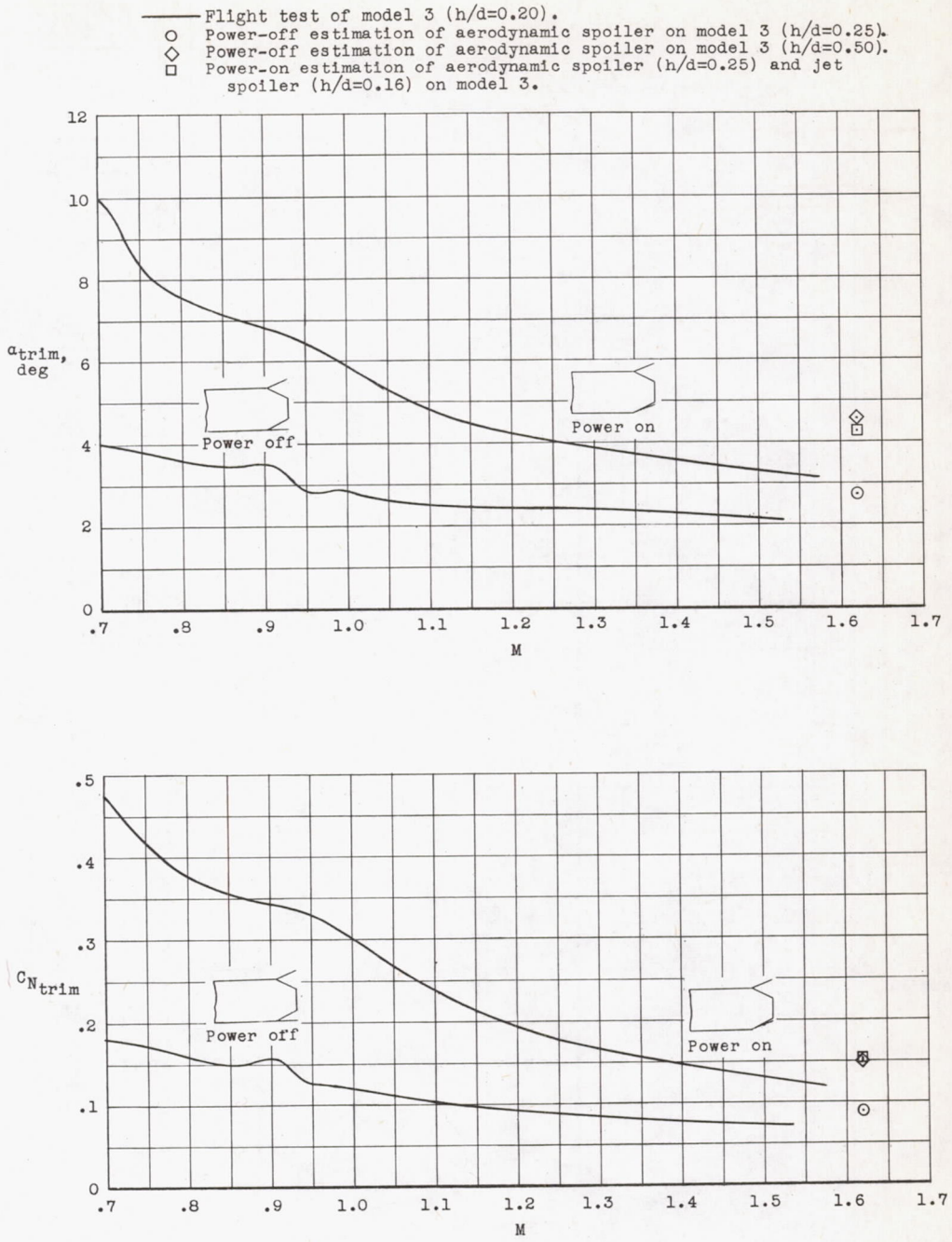

(a) Comparisons of trim angle of attack and trim normal-force coefficient for power on and power off.

Figure 19.- Comparison of flap with aerodynamic spoiler from wind-tunnel tests.

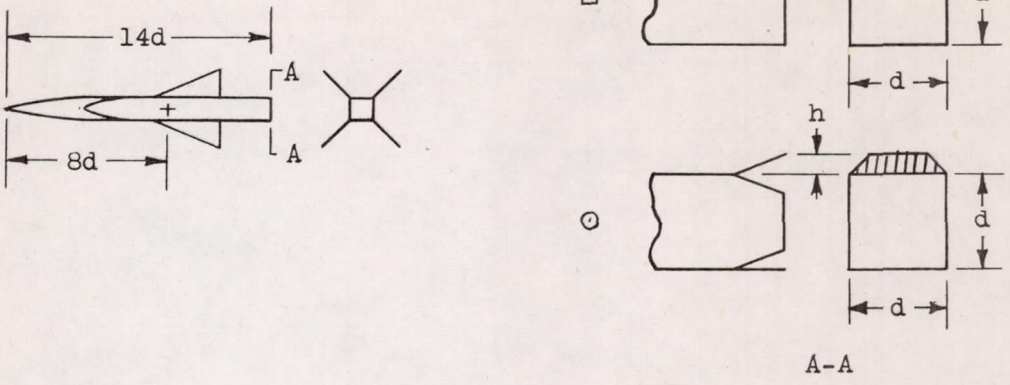

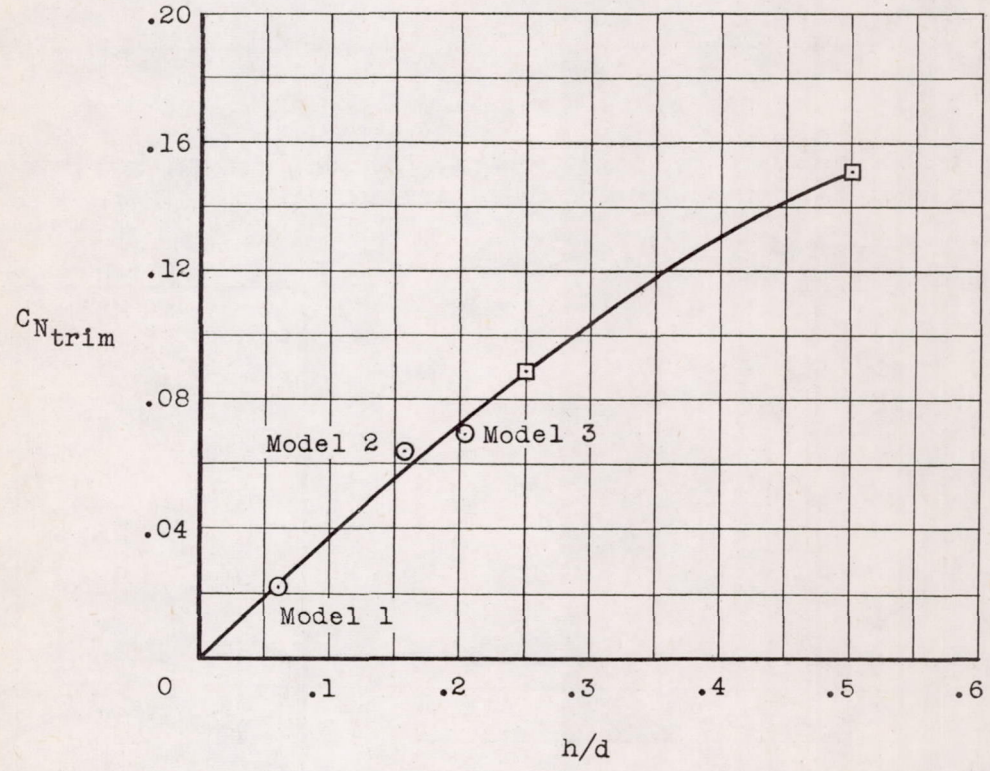

(b) Variation of trim normal-force coefficient with ratio of aerodynamic spoiler height to nozzle diameter; M = 1.62.

Figure 19.- Concluded.

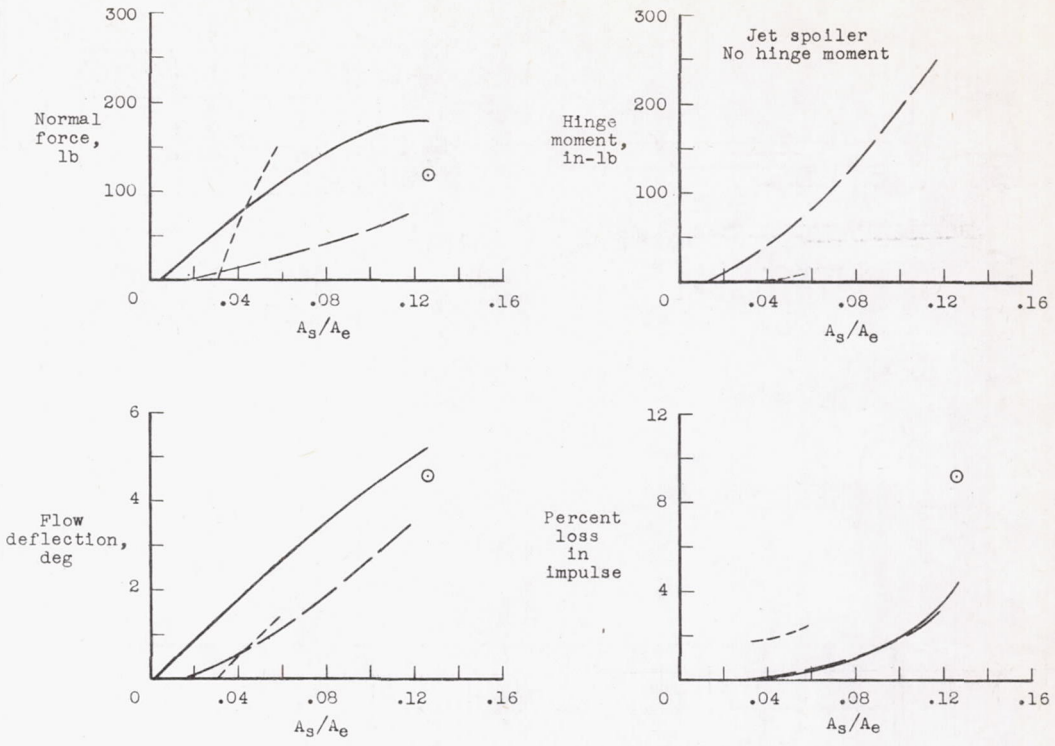

(a) Variation of normal force, hinge moment, flow deflection, and percent impulse loss with ratio of control area to jet exit area.

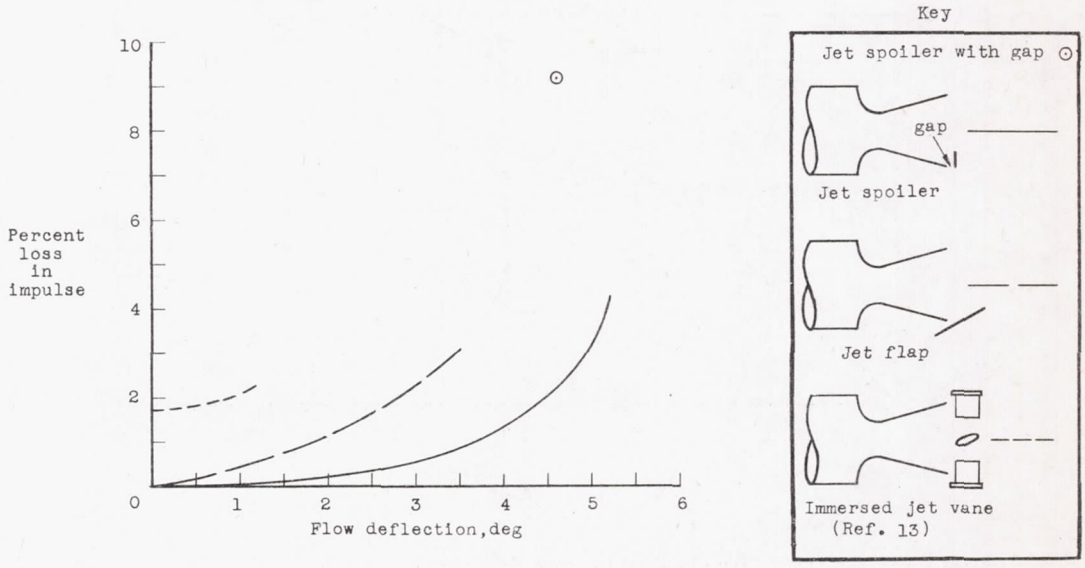

(b) Impulse loss against flow deflection.

Figure 20.- Static test comparisons for immersed jet vane, jet flap, and jet spoiler.

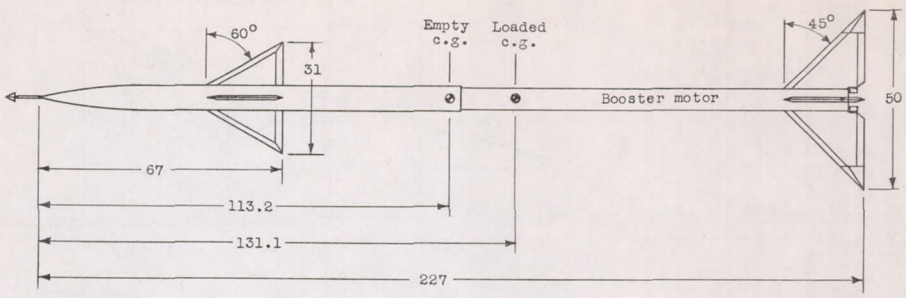

(a) Sketch of model showing center-of-gravity locations. All dimensions are in inches.

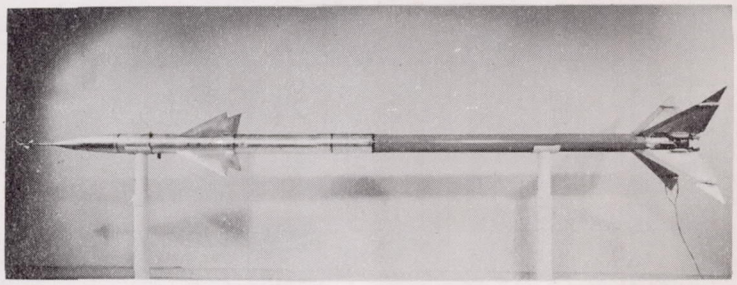

(b) Photograph of model. L-79034

GEOMETRIC CHARACTERISTICS

	Wing	Tail	Tip control	Jet vane
Total area (one plane), sq ft	2.89	4.34	0.36	0.035
Span, ft	2.58	4.16	0.60	0.104
Aspect ratio	2.30	4.00	4.00	0.625

Angular gain between tip control and jet vane is 3 to 1.

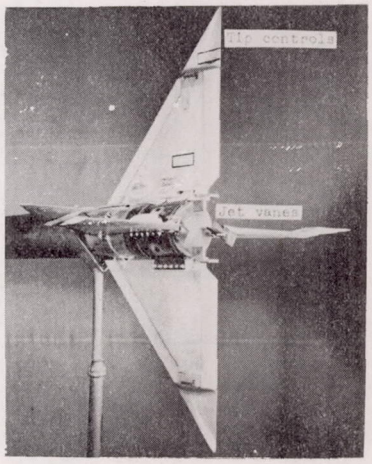

L-74879.1

(c) Photograph of tail section showing tip controls and jet vanes.

Figure 21.- Sketch, photographs, and geometric characteristics of flight model with immersed jet vanes.

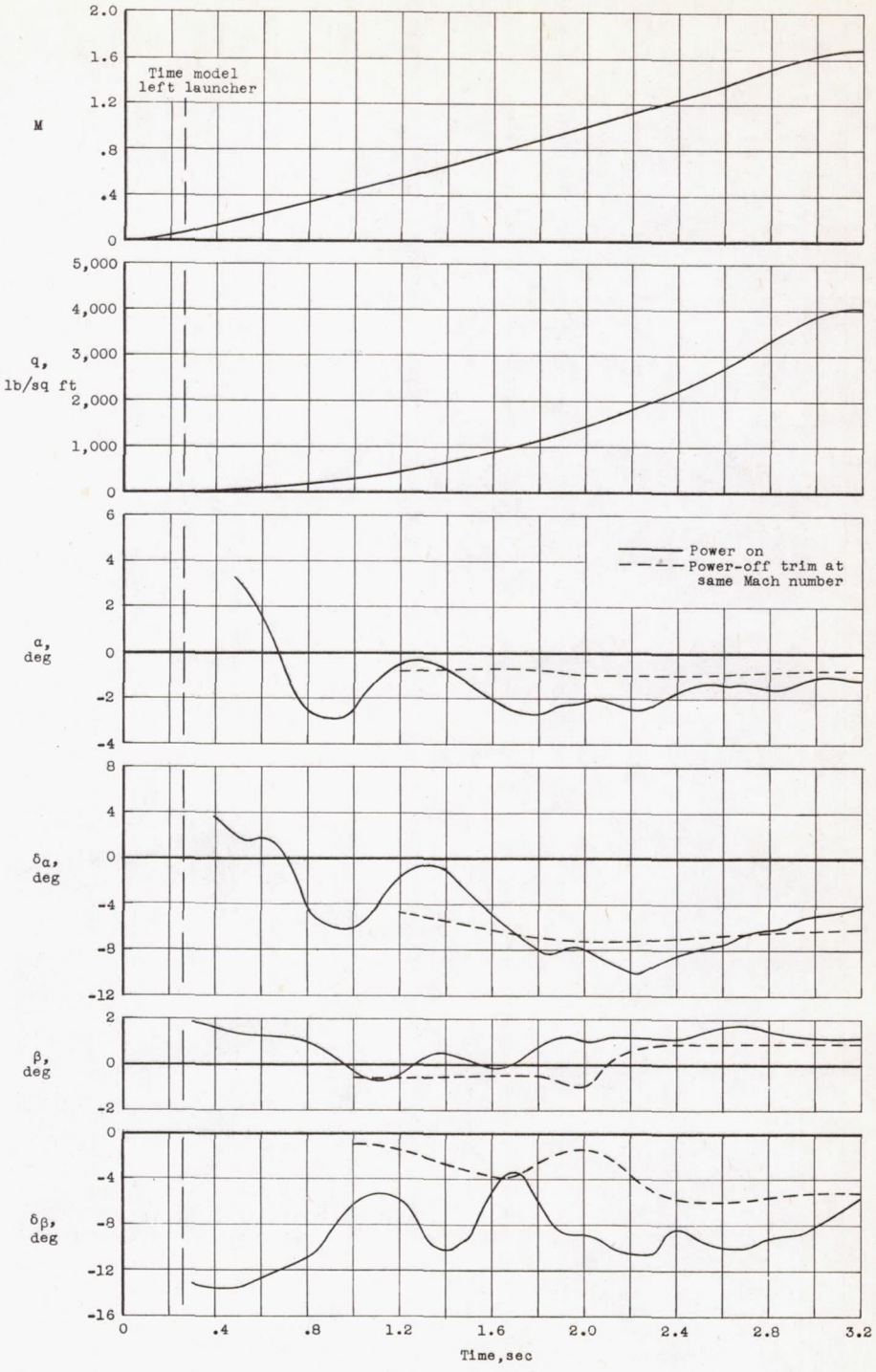

Figure 22.- Time history of power-on rocket test flight of model combining immersed jet vanes and wing tip controls.